NON-LOCAL BLIND HYPERSPECTRAL IMAGE SUPER-RESOLUTION VIA 4D SPARSE TENSOR FACTORIZATION AND LOW-RANK

Wei Wan

Laboratory of Mathematics and Complex Systems (Ministry of Education of China) School of Mathematical Sciences, Beijing Normal University Beijing 100875, China

Weihong Guo*

Department of Mathematics, Case Western Reserve University Cleveland, OH, 44106, USA

JUN LIU AND HAIYANG HUANG

Laboratory of Mathematics and Complex Systems (Ministry of Education of China) School of Mathematical Sciences, Beijing Normal University Beijing 100875, China

(Communicated by Bin Dong)

ABSTRACT. Hyperspectral image (HSI) super-resolution is a technique to improve the spatial resolution of a HSI for better visual perception and down stream applications. This is a very ill-posed inverse problem and is often solved by fusing the low-resolution (LR) HSI with a high-resolution (HR) multispectral image (MSI). It is more challenging for blind HSI super-resolution, i.e., when the spatial degradation operators are completely unknown. In this paper, we propose a novel sparse tensor factorization model for the task of blind HSI super-resolution using the spatial non-local self-similarity and spectral global correlation of HSIs. Image clustering method is employed to collect some similar 3D cubes of HSIs which can be formed as some 4D image clusters with high correlation. We conduct cluster wise computation to not only save computation time but also to introduce a non-local regularity originated from the redundancy of cubes. By using the sparsity of tensor decomposition and the low-rank in non-local self-similarity direction underlying 4D similar clusters, we design a sparse tensor regularization term, which preserves the spatial-spectral structural correlation of HSIs. In addition, we present a proximal alternating direction method of multipliers (ADMM) based algorithm to efficiently solve the proposed model. Numerical experiments demonstrate that the proposed model outperforms many state-of-the-art HSI super-resolution methods.

1. **Introduction.** A hyperspectral image (HSI) is a three-dimensional tensor with one dimension corresponding to bands providing abundant spectral information. It has attracted increasing interest and attention from researchers in remote sensing [10, 2], computer vision [26, 21, 28, 29, 16] etc.. However, HSIs often suffer from spatial resolution degradation due to various hardware limitations. HSI super-resolution is a computational algorithm that raises the spatial resolution of HSI. It is often done by fusing a low-resolution (LR) HSI with a high-resolution (HR) multispectral image (MSI) of the same scene. LR-HSI and HR-MSI have complementing properties in terms of

²⁰¹⁰ Mathematics Subject Classification. Primary: 94A08; Secondary: 68U10.

Key words and phrases. Blind Super-Resolution, Hyperspectral Imaging, Non-Local Sparse Tensor Factorization, Tensor Dictionary Learning.

^{*}Corresponding author: Weihong Guo.

resolution. The later one has higher spatial while lower spectral resolution while the former one is the opposite. Almost all HSI super-resolution work assumes the degrading operators between the low resolution image and its high resolution analog are known but in reality they are not available. It is therefore important to address the issue of blind super-resolution, the problem of simultaneously resolution enhancement and degrading operators.

Super-resolution, especially blind super-resolution is a seriously ill-posed problem. Appropriate selections of regularization plays an essential role in the success of this problem. Spatial/spectral similarity and sparsity have proven to be effective. Methods in the literature are based on either 2D matrix or 3D tensor modeling. Matrix based methods unfold the 3D multispectral and hyperspectral images into 2D matrices so that for instance each row corresponding to one spectral band at all spatial locations. Matrix decomposition and sparsity are then adopted for super-resolution. In [13], Kawakami et al. introduced a sparse matrix factorization method, which reconstructs the HSI by multiplying the learned dictionary from the HR-MSI and sparse coefficients from the LR-HSI. Wycoff et al. [31] proposed a sparse non-negative matrix factorization method that exploits both non-negativity and sparsity of HSI. In [37], Yokoya et al. proposed a coupled non-negative matrix factorization (CNMF) method for HSI super-resolution by alternately applying non-negative matrix factorization (NMF) [17] unmixing to LR-HSI and HR-MSI. However, the sparsity constraints of HSIs is not considered. In [24], Simões et al. presented a convex formulation for HSI super-resolution (known as HySure) based on vector total variation regularization, which promotes piecewise-smooth solutions with discontinuity along spectral direction. In addition, the spatial and spectral responses of the sensors are both estimated from the observed images. In [32], an adaptive sparse matrix representation method was proposed by Wei et al.. In [1], a non-parametric Bayesian sparse representation (BSR) method for the fusion of HSI and MSI was proposed by Akhtar et al.. In [6], Dong et al. proposed a clustering-based non-negative structured sparse representation approach with spatial-spectral sparsity of the HSI. In [39], Zhang et al. developed a novel clustering manifold structure based HSI super-resolution framework. The learned manifold structure from the HR-MSI can well capture the spatial correlation of the target HR-HSI.

Transforming 3D images into 2D matrices however loses spectral correlation. Tensor modeling better preserves the data structure. Recently, tensor based methods have been successfully applied to hyperspectral image processing, such as restoration [22, 4, 9, 25, 35, 36], segmentation [40], matching [20], recognition [11, 12], classification [41, 42] and unmixing [3, 19, 23]. In [7], Dian et al. proposed a non-local sparse tensor factorization (NLSTF) model for HSI super-resolution, which induces spatial dictionaries and core tensors from HR-MSI and spectral dictionaries from LR-HSI, respectively. However, this method does not combine LR-HSI and HR-MSI to estimate the dictionaries and the core tensor for each cluster. Chang et al. [4] presented a weighted low-rank tensor recovery model by using high order singular value decomposition. It updates core tensors iteratively while fixing the dictionaries along every mode. In [14], a coupled tensor factorization model was proposed by Kanatsoulis et al. to tackle the HSI and MSI fusion task when the spatial degradation operator is unknown or inaccurately estimated. This approach however didn't consider the spatial non-local self-similarity and tensor sparsity prior. Very recently, Li et al. [18] proposed a coupled sparse tensor factorization (CSTF) based HSI super-resolution model, however, without considering the non-local spatial similarity in the HSI. To incorporate non-local similarity and global correlation across spectrum, cubes based methods are adopted. Images are divided into full band patches (FBP) and grouped into clusters based on similarity. For each of the cluster, its FBPs are either organized into a 3rd order tensor by unfolding along spectral dimension [4, 36] or a 4th order tensor without any unfolding to preserve the high dimension structure [22, 7]. The computation is then done cluster by cluster. In this work, we adopt 4th order tensor modeling to best preserve the data structure.

The majority of the hyperspectral super-resolution work assumes the spatial degrading operator is known or is easy to be estimated before hand. In practice, they are usually unknown or hard to be estimated accurately. In this paper, we propose a novel blind HSI super-resolution when the spatial degradation operators are completely unknown. This method combines non-local regularity and sparse tensor factorization into a unified framework. We first group similar 3D cubes into clusters using K-means ++. The similar cubes in each cluster are organized in a 4th order tensor and represented using Tucker decomposition. The HSI super-resolution problem can be changed to calculate the spatial and spectral dictionaries of three modes and the corresponding core tensor for each cluster. Moreover, a new tensor sparsity measure is designed, and it can be easily extended to many other problems. Furthermore, an effective proximal ADMM based algorithm is proposed

to solve the blind HSI super-resolution problem. Numerical experiments show that the proposed approach provides impressive blind HSI super-resolution results.

The rest of the paper is organized as follows. In Section 2, we briefly introduce basis notations and review some preliminaries on tensors. We present the proposed HSI super-resolution model in Section 3. In Section 4, we show the blind algorithm and some details about the implementation. Experimental results are laid out in Section 5 and conclusion follows in Section 6.

2. Notations and preliminaries. Let $\mathcal{X} \in \mathbb{R}^{I_1 \times I_2 \cdots \times I_N}$ be an N^{th} -order real valued tensor and x_{i_1,i_2,\cdots,i_N} be its (i_1,i_2,\cdots,i_N) -element. Then the corresponding l_1 norm is defined as $\|\mathcal{X}\|_1 = \sum_{\substack{i_1,i_2,\cdots,i_N \\ i_1,i_2,\cdots,i_N}} |x_{i_1,i_2,\cdots,i_N}|$, and the $Frobenius\ norm$ of \mathcal{X} is calculated by $\|\mathcal{X}\|_F = \sqrt{\sum_{\substack{i_1,i_2,\cdots,i_N \\ i_1,i_2,\cdots,i_N}} x_{i_1,i_2,\cdots,i_N}^2}$. $\|\mathcal{X}\|_0$ denote the l_0 semi-norm counting the number of non-zero elements in \mathcal{X} .

The mode-n vectors of a tensor $\mathcal X$ are those obtained by fixing every index except the n-th one. For instance, mode-1 vectors are $\mathcal X(1:I_1,1,\cdots,1),\ \mathcal X(1:I_1,1,\cdots,2),$ etc. The mode-n matricization, also known as the unfolding or flattening, of a tensor $\mathcal X\in\mathbb R^{I_1\times I_2\cdots\times I_N}$ is the matrix denoted as $\mathbf X_{(n)}\equiv \mathrm{unfold}_n(\mathcal X)\in\mathbb R^{I_n\times (I_1\cdots I_{n-1}I_{n+1}\cdots I_N)}$ and obtained by arranging the mode-n vectors to be the columns. The n-mode product of a tensor $\mathcal X\in\mathbb R^{I_1\times I_2\cdots\times I_N}$ with a matrix $\mathbf U\in\mathbb R^{J\times I_n}$ is denoted by $\mathcal X\times_n\mathbf U\in\mathbb R^{I_1\times\cdots\times I_{n-1}\times J\times I_{n+1}\times\cdots\times I_N}$, with entries

(1)
$$(\mathcal{X} \times_n \mathbf{U})_{i_1 \cdots i_{n-1} j i_{n+1} \cdots i_N} = \sum_{i_n=1}^{I_n} x_{i_1 i_2 \cdots i_N} u_{j i_n}.$$

Besides, the *n*-mode product can also be calculated by the matrix multiplication:

(2)
$$\mathcal{Y} = \mathcal{X} \times_n \mathbf{U} \Leftrightarrow \mathbf{Y}_{(n)} = \mathbf{U} \mathbf{X}_{(n)}.$$

For distinct/same mode multiplication, we have

$$\mathcal{X} \times_m \mathbf{A} \times_n \mathbf{B} = \mathcal{X} \times_n \mathbf{B} \times_m \mathbf{A} (m \neq n),$$

 $\mathcal{X} \times_n \mathbf{A} \times_n \mathbf{B} = \mathcal{X} \times_n (\mathbf{B} \mathbf{A}).$

Definition 2.1 (Tucker Decomposition). Tucker decomposition of an N^{th} -order tensor $\mathcal{X} \in \mathbb{R}^{I_1 \times I_2 \cdots \times I_N}$ can be written as

(3)
$$\mathcal{X} = \mathcal{Y} \times_1 \mathbf{A}_1 \times_2 \mathbf{A}_2 \cdots \times_N \mathbf{A}_N.$$

Here, $\mathbf{A}_n \in \mathbb{R}^{I_n \times M_n}$ are the factor matrices along mode n and $\mathcal{Y} \in \mathbb{R}^{M_1 \times M_2 \cdots \times M_N}$ is called the core tensor.

Let the vectorization of a tensor \mathcal{X} be defined as $vec(\mathcal{X}) \equiv vec(\mathbf{X}_{(1)}) \in \mathbb{R}^{I_1 I_2 \cdots I_N}$, i.e. the long vector obtained by stacking all the mode-1 vectors vertically. The mode-n unfolding of the Tucker decomposition (3) is [15]:

(4)
$$\mathbf{X}_{(n)} = \mathbf{A}_n \mathbf{Y}_{(n)} (\mathbf{A}_N \otimes \cdots \otimes \mathbf{A}_{n+1} \otimes \mathbf{A}_{n-1} \otimes \cdots \otimes \mathbf{A}_1)^T,$$

and its vector representation [5] is

(5)
$$\mathbf{x} = (\mathbf{A}_N \otimes \mathbf{A}_{N-1} \otimes \cdots \otimes \mathbf{A}_1)\mathbf{y},$$

where $\mathbf{x} = vec(\mathcal{X})$, $\mathbf{y} = vec(\mathcal{Y})$ and the symbol " \otimes " denotes the *Kronecker product* of matrices, which has the following properties that will prove useful in our discussions:

$$(\mathbf{A} \otimes \mathbf{B})(\mathbf{C} \otimes \mathbf{D}) = \mathbf{AC} \otimes \mathbf{BD},$$
$$(\mathbf{A} \otimes \mathbf{B})^T = \mathbf{A}^T \otimes \mathbf{B}^T.$$

3. The proposed method. Let $\mathcal{X} \in \mathbb{R}^{W \times H \times S}$ be the target HR-HSI to be recovered, where W, H and S denote the dimensions of the width, height and spectral mode, respectively. The tensor $\mathcal{Y} \in \mathbb{R}^{w \times h \times S}$ denotes the corresponding LR-HSI, and $\mathcal{Z} \in \mathbb{R}^{W \times H \times s}$ denotes the HR-MSI of the same scene, where w < W, h < H and s < S. The purpose of HSI super-resolution is to estimate the HR-HSI \mathcal{X} by fusing the LR-HSI \mathcal{Y} with the HR-MSI \mathcal{Z} as illustrated in Figure 1. Reconstructing \mathcal{X} from \mathcal{Y} , \mathcal{Z} when there is noise is an ill-posed inverse problem. When there no knowledge of the downgrading matrices, it is more difficult.

Due to modeling accuracy and large size of the data, the computation is usually not done on the entire domain but on clusters of small cubes. Clustering similar cubes together and

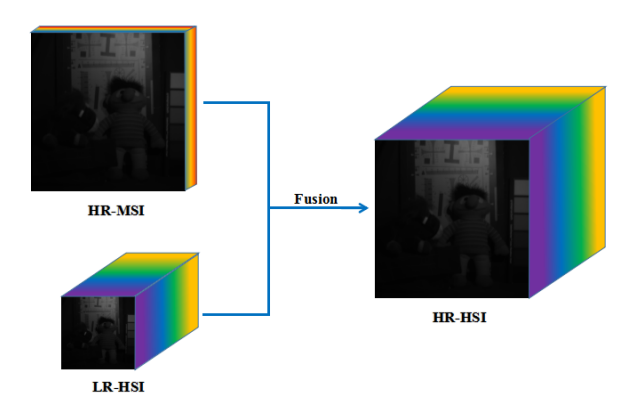


FIGURE 1. Illustration of the hyperspectral image super-resolution task.

conducting cluster wise computation not only save computation but also bring non-local regularity. A collection of various similar high dimensional cubes leads to a natural high order tensor. We will adopt high order tensor decomposition to better model the similarity among cubes. We divide the HR-MSI \mathcal{Z} into 3D cubes $\{\mathcal{Z}_i\}_{i=1}^n\subset\mathbb{R}^{d_W\times d_H\times s}$ with overlaps, where d_W and d_H denote the spatial width and height dimensions, the overlaps along two spatial modes are $l_w=d_W/2$ and $l_h=d_H/2$, respectively, $n=n_wn_h$ is the number of cubes and $n_w=(W-l_w)/(d_W-l_w), n_h=(H-l_h)/(d_H-l_h)$. Similarly, we create another set of small 3D cubes $\{\mathcal{Y}_i\}_{i=1}^n\subset\mathbb{R}^{d_w\times d_h\times S}$ from the LR-HSI \mathcal{Y} in the same way, where $d_w=d_W/a, d_s=d_H/a, a$ is the scaling factor (e.g. in this work, we set $a=8, d_W=d_H=16, d_w=d_h=2$). Then all the 3D cubes of the HR-MSI \mathcal{Z} can be grouped into K clusters $\{\mathcal{Z}^{(k,j)}\}_{j=1}^{n_k}$ ($k=1,2,\cdots,K$) by K-means++, where K is the number of clusters, n_k is the number of cubes in the k^{th} cluster and $\mathcal{Z}^{(k,j)}$ denotes the j^{th} cube of the k^{th} cluster. Furthermore, the similar cubes in the k^{th} cluster can be organized as a k^{th} order tensor: k^{th} cluster. Furthermore, the similar cubes in the k^{th} cluster can be organized as a k^{th} order tensor: k^{th} cluster. Furthermore, the similar cubes in the k^{th} cluster can be organized as a k^{th} order tensor: k^{th} cluster. Furthermore, the similar cubes in the k^{th} cluster can be organized as a k^{th} order tensor: k^{th} cluster. Furthermore, the similar cubes in the k^{th} cluster can be organized as a k^{th} order tensor: k^{th} cluster. Furthermore, the similar cubes in the k^{th} cluster can be organized as a k^{th} order tensor: k^{th} cluster. Furthermore, the similar cubes in the k^{th} cluster can be organized as a k^{th} order tensor: k^{th} cluster. Furthermore, the similar cubes in the k^{th} cluster can be organi

For the k^{th} cluster, when there is no noise, the acquired $\mathcal{Y}^{(k)}$ is the spatially downsampled version of $\mathcal{X}^{(k)}$,

$$\mathcal{Y}^{(k)} = \mathcal{X}^{(k)} \times_1 \mathbf{P}_1 \times_2 \mathbf{P}_2,$$

where $\mathbf{P}_1 \in \mathbb{R}^{d_W \times d_W}$ and $\mathbf{P}_2 \in \mathbb{R}^{d_h \times d_H}$ are the blurring and downsampling matrices along the width (first) mode and height (second) mode, respectively. In this work, \mathbf{P}_1 and \mathbf{P}_2 are both completely unknown. Besides, $\mathcal{Z}^{(k)}$ is the spectrally downsampled version of $\mathcal{X}^{(k)}$.

$$\mathcal{Z}^{(k)} = \mathcal{X}^{(k)} \times_3 \mathbf{P}_3,$$

where $\mathbf{P}_3 \in \mathbb{R}^{s \times S}$ is the downsampled matrix of the spectral (third) mode. Based on Tucker decomposition, the kth cluster $\mathcal{X}^{(k)}$ of the HR-HSI \mathcal{X} can be formulated as

(6)
$$\mathcal{X}^{(k)} = \mathcal{C}^{(k)} \times_1 \mathbf{W}_k \times_2 \mathbf{H}_k \times_3 \mathbf{S}_k,$$

where the matrices $\mathbf{W}_k \in \mathbb{R}^{d_W \times r_k^W}$, $\mathbf{H}_k \in \mathbb{R}^{d_H \times r_k^H}$ and $\mathbf{S}_k \in \mathbb{R}^{S \times r_k^S}$ denote the dictionaries of the width, height and spectral mode, respectively, and the tensor $\mathcal{C}^{(k)} \in \mathbb{R}^{r_k^W \times r_k^H \times r_k^S \times n_k}$ is the coefficient of $\mathcal{X}^{(k)}$ over the three dictionaries.

The proposed tensor sparsity measure for $\mathcal{X}^{(k)}$ is defined as

$$S(\mathcal{X}^{(k)}) = \lambda_c \|\mathcal{C}^{(k)}\|_0 + \mu \operatorname{rank}(X_{(4)}^{(k)}),$$

where $X_{(4)}^{(k)}$ is the unfolding along mode-4, λ_c and μ are two positive parameters. The first term enforces sparsity under Tucker decomposition. The second term originates from the fact that the cubes in the cluster have some self-similarity/correlation that will leads to low-rank of $X_{(4)}^{(k)}$.

The minimization problem with l_0 semi-norm and rank terms is non-convex. In order to simplify the computation, we replace the l_0 semi-norm by the l_1 norm and the rank with the nuclear norm,

$$S^*(\mathcal{X}^{(k)}) = \lambda_c \|\mathcal{C}^{(k)}\|_1 + \mu \|X_{(4)}^{(k)}\|_*,$$

where $\|\cdot\|_*$ is the nuclear norm defined as the sum of the singular values of $X_{(4)}^{(k)}$.

4. **Blind algorithm.** Since the spatial degradation operators \mathbf{P}_1 and \mathbf{P}_2 are unknown in practice, we design a blind super-resolution algorithm to solve the proposed model. Representing $\mathcal{X}^{(k)}$ in terms of Tucker decomposition, the proposed model is:

(7)
$$\min_{\mathcal{C}^{(k)}, \mathbf{W}_{k}, \mathbf{H}_{k}, \mathbf{S}_{k}} \frac{1}{2} \| \mathcal{Y}^{(k)} - \mathcal{C}^{(k)} \times_{1} (\mathbf{P}_{1} \mathbf{W}_{k}) \times_{2} (\mathbf{P}_{2} \mathbf{H}_{k}) \times_{3} \mathbf{S}_{k} \|_{F}^{2} \\
+ \frac{\lambda_{1}}{2} \| \mathcal{Z}^{(k)} - \mathcal{C}^{(k)} \times_{1} \mathbf{W}_{k} \times_{2} \mathbf{H}_{k} \times_{3} (\mathbf{P}_{3} \mathbf{S}_{k}) \|_{F}^{2} + \lambda_{c} \| \mathcal{C}^{(k)} \|_{1} + \mu \| X_{(4)}^{(k)} \|_{*}.$$

We solve the above minimization problem by introducing three auxiliary variables $\mathcal{M}^{(k)} = \mathcal{X}^{(k)} = \mathcal{C}^{(k)} \times_1 \mathbf{W}_k \times_2 \mathbf{H}_k \times_3 \mathbf{S}_k, \mathbf{W}_k^* = \mathbf{P}_1 \mathbf{W}_k, \mathbf{H}_k^* = \mathbf{P}_2 \mathbf{H}_k$ and forming an approximated problem:

$$\min_{\mathcal{C}^{(k)}, \mathbf{W}_{k}, \mathbf{H}_{k}, \mathbf{S}_{k}, \mathbf{W}_{k}^{*}, \mathbf{H}_{k}^{*}, \mathcal{M}^{(k)}} \frac{1}{2} \| \mathcal{Y}^{(k)} - \mathcal{C}^{(k)} \times_{1} \mathbf{W}_{k}^{*} \times_{2} \mathbf{H}_{k}^{*} \times_{3} \mathbf{S}_{k} \|_{F}^{2}
+ \frac{\lambda_{1}}{2} \| \mathcal{Z}^{(k)} - \mathcal{C}^{(k)} \times_{1} \mathbf{W}_{k} \times_{2} \mathbf{H}_{k} \times_{3} \mathbf{P}_{3} \mathbf{S}_{k} \|_{F}^{2} + \lambda_{c} \| \mathcal{C}^{(k)} \|_{1} + \mu \| M_{(4)}^{(k)} \|_{*},
+ \frac{\beta_{1}}{2} \| \mathbf{W}_{k}^{*} - \mathbf{P}_{1} \mathbf{W}_{k} \|_{F}^{2} + \frac{\beta_{2}}{2} \| \mathbf{H}_{k}^{*} - \mathbf{P}_{2} \mathbf{H}_{k} \|_{F}^{2},
(8) \qquad s.t. \ \mathcal{C}^{(k)} \times_{1} \mathbf{W}_{k} \times_{2} \mathbf{H}_{k} \times_{3} \mathbf{S}_{k} - \mathcal{M}^{(k)} = 0,$$

where $M_{(4)}^{(k)} = \text{unfold}_4(\mathcal{M}^{(k)})$. Then its augmented Lagrangian function is with the form:

$$L(\mathcal{C}^{(k)}, \mathbf{W}_{k}, \mathbf{H}_{k}, \mathbf{S}_{k}, \mathbf{W}_{k}^{*}, \mathbf{H}_{k}^{*}, \mathbf{P}_{1}, \mathbf{P}_{2}, \mathcal{M}^{(k)}, \mathcal{P}^{(k)})$$

$$= \frac{1}{2} \|\mathcal{Y}^{(k)} - \mathcal{C}^{(k)} \times_{1} \mathbf{W}_{k}^{*} \times_{2} \mathbf{H}_{k}^{*} \times_{3} \mathbf{S}_{k}\|_{F}^{2}$$

$$+ \frac{\lambda_{1}}{2} \|\mathcal{Z}^{(k)} - \mathcal{C}^{(k)} \times_{1} \mathbf{W}_{k} \times_{2} \mathbf{H}_{k} \times_{3} \mathbf{P}_{3} \mathbf{S}_{k}\|_{F}^{2} + \lambda_{c} \|\mathcal{C}^{(k)}\|_{1} + \mu \|M_{(4)}^{(k)}\|_{*}$$

$$+ \frac{\beta_{1}}{2} \|\mathbf{W}_{k}^{*} - \mathbf{P}_{1} \mathbf{W}_{k}\|_{F}^{2} + \frac{\beta_{2}}{2} \|\mathbf{H}_{k}^{*} - \mathbf{P}_{2} \mathbf{H}_{k}\|_{F}^{2},$$

$$+ \frac{\lambda_{2}}{2} \|\mathcal{M}^{(k)} - \mathcal{C}^{(k)} \times_{1} \mathbf{W}_{k} \times_{2} \mathbf{H}_{k} \times_{3} \mathbf{S}_{k} - \mathcal{P}^{(k)}\|_{F}^{2},$$

$$(9)$$

where $\mathcal{P}^{(k)}$ is the Lagrange multiplier and λ_2 is a positive parameter. For better convergence, we solve the problem under the proximal ADMM framework. We alternate some subproblems iteratively and each subproblem can be updated as follows.

4.1. $C^{(k)}$ subproblem. With the other parameters fixed, $C^{(k)}$ can be updated by solving

$$\min_{\mathcal{C}^{(k)}} \frac{1}{2} \| \mathcal{Y}^{(k)} - \mathcal{C}^{(k)} \times_{1} \mathbf{W}_{k}^{*} \times_{2} \mathbf{H}_{k}^{*} \times_{3} \mathbf{S}_{k} \|_{F}^{2}
+ \frac{\lambda_{1}}{2} \| \mathcal{Z}^{(k)} - \mathcal{C}^{(k)} \times_{1} \mathbf{W}_{k} \times_{2} \mathbf{H}_{k} \times_{3} \mathbf{P}_{3} \mathbf{S}_{k} \|_{F}^{2}
+ \frac{\lambda_{2}}{2} \| \mathcal{O}^{(k)} - \mathcal{C}^{(k)} \times_{1} \mathbf{W}_{k} \times_{2} \mathbf{H}_{k} \times_{3} \mathbf{S}_{k} \|_{F}^{2}
+ \lambda_{c} \| \mathcal{C}^{(k)} \|_{1} + \frac{\sigma}{2} \| \mathcal{C}^{(k)} - \mathcal{C}^{(k)}_{pre} \|_{F}^{2}, \tag{10}$$

where $\mathcal{O}^{(k)} = \mathcal{M}^{(k)} - \mathcal{P}^{(k)}$ and $\mathcal{C}^{(k)}_{pre}$ represents the estimated $\mathcal{C}^{(k)}$ in the previous iteration. Furthermore, since $C^{(k)}$ contains n_k cubes, the above problem can be equivalently reformulated as

$$\min_{\mathcal{C}^{(k,j)}} \frac{1}{2} \sum_{j=1}^{n_k} \| \mathcal{Y}^{(k,j)} - \mathcal{C}^{(k,j)} \times_1 \mathbf{W}_k^* \times_2 \mathbf{H}_k^* \times_3 \mathbf{S}_k \|_F^2
+ \frac{\lambda_1}{2} \sum_{j=1}^{n_k} \| \mathcal{Z}^{(k,j)} - \mathcal{C}^{(k,j)} \times_1 \mathbf{W}_k \times_2 \mathbf{H}_k \times_3 \mathbf{P}_3 \mathbf{S}_k \|_F^2
+ \frac{\lambda_2}{2} \sum_{j=1}^{n_k} \| \mathcal{O}^{(k,j)} - \mathcal{C}^{(k,j)} \times_1 \mathbf{W}_k \times_2 \mathbf{H}_k \times_3 \mathbf{S}_k \|_F^2
+ \lambda_c \| \mathcal{C}^{(k)} \|_1 + \frac{\sigma}{2} \| \mathcal{C}^{(k)} - \mathcal{C}^{(k)}_{pre} \|_F^2,$$
(11)

According to the relationship between the Tucker model and Kronecker representation (equation (5)), the above problem can be formulated as

$$\min_{\mathbf{C}^{(k)}} \frac{1}{2} \| \mathbf{Y}^{(k)} - \mathbf{D}_1 \mathbf{C}^{(k)} \|_F^2 + \frac{\lambda_1}{2} \| \mathbf{Z}^{(k)} - \mathbf{D}_2 \mathbf{C}^{(k)} \|_F^2 + \frac{\lambda_2}{2} \| \mathbf{O}^{(k)} - \mathbf{D}_3 \mathbf{C}^{(k)} \|_F^2 + \frac{\lambda_2}{2} \| \mathbf{O}^{(k)} - \mathbf{O}_3 \mathbf{C}^{(k)$$

where $\mathbf{C}^{(k)} = [\mathbf{c}^{(k,1)}, \mathbf{c}^{(k,2)}, \cdots, \mathbf{c}^{(k,n_k)}], \mathbf{Y}^{(k)} = [\mathbf{y}^{(k,1)}, \mathbf{y}^{(k,2)}, \cdots, \mathbf{y}^{(k,n_k)}], \mathbf{Z}^{(k)} = [\mathbf{z}^{(k,1)}, \mathbf{z}^{(k,2)}, \cdots, \mathbf{z}^{(k,n_k)}], \mathbf{C}^{(k)} = [\mathbf{c}^{(k,1)}, \mathbf{c}^{(k,2)}, \cdots, \mathbf{c}^{(k,n_k)}], \mathbf{c}^{(k,2)} = \mathbf{c}^{(k,2)}, \mathbf{c}^{(k,2)}, \cdots, \mathbf{c}^{(k,n_k)} = \mathbf{c}^{(k,2)}, \mathbf{c}^{(k,2)}, \cdots, \mathbf{c}^{(k,n_k)}]$ are matrices, $\mathbf{c}^{(k,j)} = vec(\mathcal{C}^{(k,j)}), \mathbf{c}^{(k,j)} = vec(\mathcal{C}^{(k,j)}), \mathbf{c}^{(k,2)}, \cdots, \mathbf{c}^{(k,n_k)} = \mathbf{c}^{(k,2)}, \cdots, \mathbf{c}^{(k,2)}, \cdots, \mathbf{c}^{(k,n_k)} = \mathbf{c}^{(k,2)}, \cdots, \mathbf{c}^{(k,n_k)} = \mathbf{c}^{(k,2)}, \cdots, \mathbf{c}^{(k,2)}, \cdots$ $= vec(\mathcal{Z}^{(k,j)}), \ \mathbf{o}^{(k,j)} = vec(\mathcal{O}^{(k,j)})$ are vectors by stacking vertically all the mode-1 vectors of = $vec(\mathcal{Z}^{(k,j)})$, $\mathcal{D}^{(k,j)} = vec(\mathcal{D}^{(k,j)})$ are vectors by stacking vertically all the mode-1 vectors of tensor $\mathcal{C}^{(k,j)}, \mathcal{Y}^{(k,j)}, \mathcal{Z}^{(k,j)}$ and $\mathcal{O}^{(k,j)}$, respectively, and the matrices $\mathbf{D}_1 = \mathbf{S}_k \otimes \mathbf{H}_k^* \otimes \mathbf{W}_k^* \in \mathbb{R}^{d_w d_h S \times r_k^W r_k^H r_k^S}$, $\mathbf{D}_2 = (\mathbf{P}_3 \mathbf{S}_k) \otimes \mathbf{H}_k \otimes \mathbf{W}_k \in \mathbb{R}^{d_W d_H S \times r_k^W r_k^H r_k^S}$ and $\mathbf{D}_3 = \mathbf{S}_k \otimes \mathbf{H}_k \otimes \mathbf{W}_k \in \mathbb{R}^{d_W d_H S \times r_k^W r_k^H r_k^S}$ are the dictionaries.

To solve $\mathbf{C}^{(k)}$, we add three auxiliary variables $\mathbf{B}_1^{(k)}, \mathbf{B}_2^{(k)}$ and $\mathbf{B}_3^{(k)}$ to substitute $\mathbf{C}^{(k)}$, and

rewrite the above problem as

$$\min_{\mathbf{B}_{1}^{(k)}, \mathbf{B}_{2}^{(k)}, \mathbf{B}_{3}^{(k)}, \mathbf{C}^{(k)}} \frac{1}{2} \| \mathbf{Y}^{(k)} - \mathbf{D}_{1} \mathbf{B}_{1}^{(k)} \|_{F}^{2} + \frac{\lambda_{1}}{2} \| \mathbf{Z}^{(k)} - \mathbf{D}_{2} \mathbf{B}_{2}^{(k)} \|_{F}^{2}
+ \frac{\lambda_{2}}{2} \| \mathbf{O}^{(k)} - \mathbf{D}_{3} \mathbf{B}_{3}^{(k)} \|_{F}^{2} + \lambda_{c} \| \mathbf{C}^{(k)} \|_{1} + \frac{\sigma}{2} \| \mathbf{C}^{(k)} - \mathbf{C}_{pre}^{(k)} \|_{F}^{2},
(13) \qquad s.t. \ \mathbf{B}_{1}^{(k)} = \mathbf{C}^{(k)}, \mathbf{B}_{2}^{(k)} = \mathbf{C}^{(k)}, \mathbf{B}_{3}^{(k)} = \mathbf{C}^{(k)}.$$

Then we can use standard augmented Lagrangian method to produce the following scheme:

Then we can use standard augmented Lagrangian method to produce the following scheme
$$\begin{cases} (\mathbf{B}_{1}^{(k)}{}^{t+1}, \mathbf{B}_{2}^{(k)}{}^{t+1}, \mathbf{B}_{3}^{(k)}{}^{t+1}, \mathbf{C}^{(k)}{}^{t+1}) \\ = & \arg\min_{\mathbf{B}_{1}^{(k)}, \mathbf{B}_{2}^{(k)}, \mathbf{B}_{3}^{(k)}, \mathbf{C}^{(k)} \end{cases} \\ + \frac{2}{2} \|\mathbf{O}^{(k)} - \mathbf{D}_{3} \mathbf{B}_{3}^{(k)} \|_{F}^{2} + \frac{\eta_{c_{1}}}{2} \|\mathbf{B}_{1}^{(k)}{}^{t+1} - \mathbf{C}^{(k)} - \mathbf{V}_{1}^{t} \|_{F}^{2} + \frac{\eta_{c_{2}}}{2} \|\mathbf{B}_{2}^{(k)}{}^{t+1} - \mathbf{C}^{(k)} - \mathbf{V}_{2}^{t} \|_{F}^{2} \\ + \frac{\eta_{c_{3}}}{2} \|\mathbf{B}_{3}^{(k)}{}^{t+1} - \mathbf{C}^{(k)} - \mathbf{V}_{3}^{t} \|_{F}^{2} + \lambda_{c} \|\mathbf{C}^{(k)}\|_{1} + \frac{\sigma}{2} \|\mathbf{C}^{(k)} - \mathbf{C}_{pre}^{(k)} \|_{F}^{2} \end{cases}, \\ \mathbf{V}_{1}^{t+1} = \mathbf{V}_{1}^{t} + (\mathbf{C}^{(k)}{}^{t+1} - \mathbf{B}_{1}^{(k)}{}^{t+1}), \\ \mathbf{V}_{2}^{t+1} = \mathbf{V}_{2}^{t} + (\mathbf{C}^{(k)}{}^{t+1} - \mathbf{B}_{2}^{(k)}{}^{t+1}), \\ \mathbf{V}_{3}^{t+1} = \mathbf{V}_{3}^{t} + (\mathbf{C}^{(k)}{}^{t+1} - \mathbf{B}_{3}^{(k)}{}^{t+1}), \end{cases}$$

By applying an alternating minimization algorithm, (14) becomes

(15)
$$\begin{cases} \mathbf{B}^{(k)^{t+1}} = \underset{\mathbf{B}^{(k)}}{\min} \left\{ \frac{1}{2} \| \mathbf{U}^{(k)} - \mathbf{D} \mathbf{B}^{(k)} \|_F^2 + \frac{1}{2} \| \mathbf{B}^{(k)} - \mathbf{C}_*^{(k)^t} - \mathbf{V}^t \|_F^2 \right\}, \\ \mathbf{C}^{(k)^{t+1}} = \underset{\mathbf{C}^{(k)}}{\min} \left\{ \frac{\eta_{c_1}}{2} \| \mathbf{B}_1^{(k)^{t+1}} - \mathbf{C}^{(k)} - \mathbf{V}_1^t \|_F^2 + \frac{\eta_{c_2}}{2} \| \mathbf{B}_2^{(k)^{t+1}} - \mathbf{C}^{(k)} - \mathbf{V}_2^t \|_F^2 + \frac{\eta_{c_3}}{2} \| \mathbf{B}_3^{(k)^{t+1}} - \mathbf{C}^{(k)} - \mathbf{V}_3^t \|_F^2 + \lambda_c \| \mathbf{C}^{(k)} \|_1 + \frac{\sigma}{2} \| \mathbf{C}^{(k)} - \mathbf{C}_{pre}^{(k)} \|_F^2 \right\}, \\ \mathbf{V}^{t+1} = \mathbf{V}^t + (\mathbf{C}_*^{(k)^{t+1}} - \mathbf{B}^{(k)^{t+1}}), \end{cases}$$

where
$$\mathbf{U}^{(k)} = \begin{bmatrix} \mathbf{Y}^{(k)} \\ \sqrt{\lambda_1} \mathbf{Z}^{(k)} \\ \sqrt{\lambda_2} \mathbf{O}^{(k)} \end{bmatrix}$$
, $\mathbf{V} = \begin{bmatrix} \sqrt{\eta_{c_1}} \mathbf{V}_1 \\ \sqrt{\eta_{c_2}} \mathbf{V}_2 \\ \sqrt{\eta_{c_3}} \mathbf{V}_3 \end{bmatrix}$, $\mathbf{B}^{(k)} = \begin{bmatrix} \sqrt{\eta_{c_1}} \mathbf{B}_1^{(k)} \\ \sqrt{\eta_{c_2}} \mathbf{B}_2^{(k)} \\ \sqrt{\eta_{c_3}} \mathbf{B}_3^{(k)} \end{bmatrix}$, $\mathbf{D} = \begin{bmatrix} \frac{1}{\sqrt{\eta_{c_1}}} \mathbf{D}_1 & 0 & 0 \\ 0 & \frac{\sqrt{\lambda_1}}{\sqrt{\eta_{c_2}}} \mathbf{D}_2 & 0 \\ 0 & 0 & \frac{\sqrt{\lambda_2}}{\sqrt{\eta_{c_3}}} \mathbf{D}_3 \end{bmatrix}$ and $\mathbf{C}_*^{(k)} = \begin{bmatrix} \sqrt{\eta_{c_1}} \mathbf{C}^{(k)} \\ \sqrt{\eta_{c_2}} \mathbf{C}^{(k)} \\ \sqrt{\eta_{c_3}} \mathbf{C}^{(k)} \end{bmatrix}$.

, it can be solved by soft thresholding

(16)
$$\mathbf{C}^{(k)}^{t+1} = \mathcal{S}(b, \frac{\lambda_c}{a}),$$

where $a = \eta_{c_1} + \eta_{c_2} + \eta_{c_3} + \sigma$, $b = \frac{1}{a} [\eta_{c_1} (\mathbf{B}_1^{(k)}^{t+1} - \mathbf{V}_1^t) + \eta_{c_2} (\mathbf{B}_2^{(k)}^{t+1} - \mathbf{V}_2^t) + \eta_{c_3} (\mathbf{B}_3^{(k)}^{t+1} - \mathbf{V}_3^t) + \sigma \mathbf{C}_{pre}^{(k)}]$ and $S(f, \mu) = \frac{f}{|f|} max\{|f| - \mu, 0\}$.

2) For $\mathbf{B}^{(k)}^{t+1}$, it has a closed-form solution:

(17)
$$\mathbf{B}^{(k)}^{t+1} = (\mathbf{D}^T \mathbf{D} + \mathbf{I})^{-1} (\mathbf{D}^T \mathbf{U}^{(k)} + \mathbf{C}_*^{(k)}^t + \mathbf{V}^t),$$

where
$$\mathbf{D}^T \mathbf{D} + \mathbf{I} = \begin{bmatrix} \frac{1}{\eta_{c_1}} \mathbf{D}_1^T \mathbf{D}_1 + \mathbf{I}_1 & 0 & 0 \\ 0 & \frac{\lambda_1}{\eta_{c_2}} \mathbf{D}_2^T \mathbf{D}_2 + \mathbf{I}_2 & 0 \\ 0 & 0 & \frac{\lambda_2}{\eta_{c_3}} \mathbf{D}_3^T \mathbf{D}_3 + \mathbf{I}_3 \end{bmatrix}$$
, $\mathbf{I}, \mathbf{I}_1, \mathbf{I}_2, \mathbf{I}_3$ are identity matrices with different sizes, and $\mathbf{D}^T \mathbf{U}^{(k)} = \begin{bmatrix} \frac{1}{\sqrt{\eta_{c_1}}} \mathbf{D}_1^T \mathbf{Y}^{(k)} \\ \frac{\lambda_1}{\sqrt{\eta_{c_2}}} \mathbf{D}_2^T \mathbf{Z}^{(k)} \\ \frac{\lambda_2}{\sqrt{\eta_{c_3}}} \mathbf{D}_3^T \mathbf{O}^{(k)} \end{bmatrix}$. Since $\mathbf{D}^T \mathbf{D}$ is a very large matrix, directly calculating it will increase the computation and slow down the operation speed.

matrix, directly calculating it will increase the computation and slow down the operation speed. Therefore, problem (17) can be equivalently separated as the following three problems:

$$\begin{split} \mathbf{B}_{1}^{(k)\,t+1} &= (\mathbf{D}_{1}^{T}\mathbf{D}_{1} + \eta_{c_{1}}\mathbf{I}_{1})^{-1}(\mathbf{D}_{1}^{T}\mathbf{Y}^{(k)} + \eta_{c_{1}}\mathbf{C}^{(k)\,t} + \eta_{c_{1}}\mathbf{V}_{1}^{t}), \\ \mathbf{B}_{2}^{(k)\,t+1} &= (\lambda_{1}\mathbf{D}_{2}^{T}\mathbf{D}_{2} + \eta_{c_{2}}\mathbf{I}_{2})^{-1}(\lambda_{1}\mathbf{D}_{2}^{T}\mathbf{Z}^{(k)} + \eta_{c_{2}}\mathbf{C}^{(k)\,t} + \eta_{c_{2}}\mathbf{V}_{2}^{t}), \\ \mathbf{B}_{3}^{(k)\,t+1} &= (\lambda_{2}\mathbf{D}_{3}^{T}\mathbf{D}_{3} + \eta_{c_{3}}\mathbf{I}_{3})^{-1}(\lambda_{2}\mathbf{D}_{3}^{T}\mathbf{O}^{(k)} + \eta_{c_{3}}\mathbf{C}^{(k)\,t} + \eta_{c_{3}}\mathbf{V}_{3}^{t}). \end{split}$$

Next, we can further simplify the computation of the $\mathbf{B}_1^{(k)}, \mathbf{B}_2^{(k)}$ and $\mathbf{B}_3^{(k)}$ subproblems by using the method in [18] when $\mathbf{W}_k^{*T}\mathbf{W}_k^{*}, \mathbf{H}_k^{*T}\mathbf{H}_k^{*}, \mathbf{S}_k^T\mathbf{S}_k$ have eigenvalue decomposition $\mathbf{E}_i\Sigma_i\mathbf{E}_i^T, i=1,2.,3$ respectively, where \mathbf{E}_i is unitary, Σ_i is diagonal. Then, we can get

$$\begin{split} (\mathbf{D}_{1}^{T}\mathbf{D}_{1} + \eta_{c_{1}}\mathbf{I}_{1})^{-1} &= ((\mathbf{S}_{k} \otimes \mathbf{H}_{k}^{*} \otimes \mathbf{W}_{k}^{*})^{T}(\mathbf{S}_{k} \otimes \mathbf{H}_{k}^{*} \otimes \mathbf{W}_{k}^{*}) + \eta_{c_{1}}\mathbf{I}_{1})^{-1} \\ &= (\mathbf{S}_{k}^{T}\mathbf{S}_{k} \otimes \mathbf{H}_{k}^{*T}\mathbf{H}_{k}^{*} \otimes \mathbf{W}_{k}^{*T}\mathbf{W}_{k}^{*} + \eta_{c_{1}}\mathbf{I}_{1})^{-1} \\ &= (\mathbf{E}_{3}\boldsymbol{\Sigma}_{3}\mathbf{E}_{3}^{T} \otimes \mathbf{E}_{2}\boldsymbol{\Sigma}_{2}\mathbf{E}_{2}^{T} \otimes \mathbf{E}_{1}\boldsymbol{\Sigma}_{1}\mathbf{E}_{1}^{T} + \eta_{c_{1}}\mathbf{I}_{1})^{-1} \\ &= ((\mathbf{E}_{3} \otimes \mathbf{E}_{2} \otimes \mathbf{E}_{1})(\boldsymbol{\Sigma}_{3} \otimes \boldsymbol{\Sigma}_{2} \otimes \boldsymbol{\Sigma}_{1})(\mathbf{E}_{3}^{T} \otimes \mathbf{E}_{2}^{T} \otimes \mathbf{E}_{1}^{T}) + \eta_{c_{1}}\mathbf{I}_{1})^{-1} \\ &= (\mathbf{E}_{3} \otimes \mathbf{E}_{2} \otimes \mathbf{E}_{1})(\boldsymbol{\Sigma}_{3} \otimes \boldsymbol{\Sigma}_{2} \otimes \boldsymbol{\Sigma}_{1} + \eta_{c_{1}}\mathbf{I}_{1})^{-1}(\mathbf{E}_{3}^{T} \otimes \mathbf{E}_{2}^{T} \otimes \mathbf{E}_{1}^{T}), \end{split}$$

and

$$\begin{aligned} \mathbf{D}_{1}^{T}\mathbf{Y}^{(k)} &= [\mathbf{D}_{1}^{T}\mathbf{y}^{(k,1)}, \mathbf{D}_{1}^{T}\mathbf{y}^{(k,2)}, \cdots, \mathbf{D}_{1}^{T}\mathbf{y}^{(k,n_{k})}] \\ &= (\mathcal{Y}^{(k)} \times_{1} \mathbf{W}_{k}^{*T} \times_{2} \mathbf{H}_{k}^{*T} \times_{3} \mathbf{S}_{k}^{T})_{(4)}^{T}, \end{aligned}$$

where $\Sigma_3 \otimes \Sigma_2 \otimes \Sigma_1 + \eta_{c_1} \mathbf{I}_1$ is a diagonal matrix and its inverse is very easy to calculate, and $\mathcal{A}_{(4)}^T = \text{unfold}_4(\mathcal{A})^T$. Similarly, we set $\mathbf{S}_k^* = \mathbf{P}_3 \mathbf{S}_k$ and $\widetilde{\mathbf{E}}_i, \widetilde{\Sigma}_i$, for i = 1, 2, 3, are unitary matrices and non-negative diagonal matrices holding the eigenvectors and eigenvalues of $\mathbf{W}_k{}^T\mathbf{W}_k, \mathbf{H}_k{}^T\mathbf{H}_k$ and $\mathbf{S}_{k}^{*T}\mathbf{S}_{k}^{*}$, respectively. Then, we have

$$(\lambda_1 \mathbf{D}_2^T \mathbf{D}_2 + \eta_{c_2} \mathbf{I})^{-1} = (\widetilde{\mathbf{E}}_3 \otimes \widetilde{\mathbf{E}}_2 \otimes \widetilde{\mathbf{E}}_1)(\lambda_1 \widetilde{\Sigma}_3 \otimes \widetilde{\Sigma}_2 \otimes \widetilde{\Sigma}_1 + \eta_{c_2} \mathbf{I})^{-1} (\widetilde{\mathbf{E}}_3^T \otimes \widetilde{\mathbf{E}}_2^T \otimes \widetilde{\mathbf{E}}_1^T),$$

$$(\lambda_2 \mathbf{D}_3^T \mathbf{D}_3 + \eta_{c_3} \mathbf{I})^{-1} = (\mathbf{E}_3 \otimes \widetilde{\mathbf{E}}_2 \otimes \widetilde{\mathbf{E}}_1)(\lambda_2 \Sigma_3 \otimes \widetilde{\Sigma}_2 \otimes \widetilde{\Sigma}_1 + \eta_{c_3} \mathbf{I})^{-1} (\mathbf{E}_3^T \otimes \widetilde{\mathbf{E}}_2^T \otimes \widetilde{\mathbf{E}}_1^T),$$

346

and

$$\begin{aligned} \mathbf{D}_{2}^{T}\mathbf{Z}^{(k)} &= (\mathcal{Z}^{(k)} \times_{1} \mathbf{W}_{k}^{T} \times_{2} \mathbf{H}_{k}^{T} \times_{3} \mathbf{S}_{k}^{*T})_{(4)}^{T}, \\ \mathbf{D}_{3}^{T}\mathbf{O}^{(k)} &= (\mathcal{O}^{(k)} \times_{1} \mathbf{W}_{k}^{T} \times_{2} \mathbf{H}_{k}^{T} \times_{3} \mathbf{S}_{k}^{T})_{(4)}^{T}. \end{aligned}$$

4.2. \mathbf{W}_k subproblem. With the other parameters fixed, \mathbf{W}_k can be updated by solving

(18)
$$\begin{aligned}
& \min_{\mathbf{W}_{k}} \frac{\lambda_{1}}{2} \| \mathcal{Z}^{(k)} - \mathcal{C}^{(k)} \times_{1} \mathbf{W}_{k} \times_{2} \mathbf{H}_{k} \times_{3} \mathbf{P}_{3} \mathbf{S}_{k} \|_{F}^{2} \\
& + \frac{\lambda_{2}}{2} \| \mathcal{O}^{(k)} - \mathcal{C}^{(k)} \times_{1} \mathbf{W}_{k} \times_{2} \mathbf{H}_{k} \times_{3} \mathbf{S}_{k} \|_{F}^{2} \\
& + \frac{\beta_{1}}{2} \| \mathbf{W}_{k}^{*} - \mathbf{P}_{1} \mathbf{W}_{k} \|_{F}^{2} + \frac{\sigma}{2} \| \mathbf{W}_{k} - \mathbf{W}_{k,pre} \|_{F}^{2}.
\end{aligned}$$

Furthermore, the above problem can be rewritten in mode-1 as the following:

$$\begin{aligned} & \min_{\mathbf{W}_{k}} \frac{\lambda_{1}}{2} \| [\mathbf{Z}_{(1)}^{(k,1)}, \mathbf{Z}_{(1)}^{(k,2)}, \cdots, \mathbf{Z}_{(1)}^{(k,n_{k})}] - \mathbf{W}_{k} [\mathbf{C}_{(1)}^{(k,1)} \mathbf{Q}_{(1)}, \mathbf{C}_{(1)}^{(k,2)} \mathbf{Q}_{(1)}, \cdots, \mathbf{C}_{(1)}^{(k,n_{k})} \mathbf{Q}_{(1)}] \|_{F}^{2} \\ & + \frac{\lambda_{2}}{2} \| [\mathbf{O}_{(1)}^{(k,1)}, \mathbf{O}_{(1)}^{(k,2)}, \cdots, \mathbf{O}_{(1)}^{(k,n_{k})}] - \mathbf{W}_{k} [\mathbf{C}_{(1)}^{(k,1)} \mathbf{F}_{(1)}, \mathbf{C}_{(1)}^{(k,2)} \mathbf{F}_{(1)}, \cdots, \mathbf{C}_{(1)}^{(k,n_{k})} \mathbf{F}_{(1)}] \|_{F}^{2} \\ & + \frac{\beta_{1}}{2} \| \mathbf{W}_{k}^{*} - \mathbf{P}_{1} \mathbf{W}_{k} \|_{F}^{2} + \frac{\sigma}{2} \| \mathbf{W}_{k} - \mathbf{W}_{k,pre} \|_{F}^{2}, \end{aligned}$$

where $\mathbf{Z}_{(1)}^{(k,j)}$, $\mathbf{O}_{(1)}^{(k,j)}$ and $\mathbf{C}_{(1)}^{(k,j)}$ are mode-1 unfolding matrices of tensors $\mathcal{Z}^{(k,j)}$, $\mathcal{O}^{(k,j)}$ and $\mathcal{C}^{(k,j)}$, respectively, and $\mathbf{Q}_{(1)} = (\mathbf{P}_3\mathbf{S}_k \otimes \mathbf{H}_k)^T$, $\mathbf{F}_{(1)} = (\mathbf{S}_k \otimes \mathbf{H}_k)^T$.

In addition, we can denote $\mathbf{Z}_1 = [\mathbf{Z}_{(1)}^{(k,1)}, \mathbf{Z}_{(1)}^{(k,2)}, \cdots, \mathbf{Z}_{(1)}^{(k,n_k)}]$, $\mathbf{O}_1 = [\mathbf{O}_{(1)}^{(k,1)}, \mathbf{O}_{(1)}^{(k,2)}, \cdots, \mathbf{O}_{(1)}^{(k,n_k)}]$, $\mathbf{Q}_1 = [\mathbf{C}_{(1)}^{(k,1)}\mathbf{Q}_{(1)}, \mathbf{C}_{(1)}^{(k,2)}\mathbf{Q}_{(1)}, \cdots, \mathbf{C}_{(1)}^{(k,n_k)}\mathbf{Q}_{(1)}]$ and $\mathbf{F}_1 = [\mathbf{C}_{(1)}^{(k,1)}\mathbf{F}_{(1)}, \mathbf{C}_{(1)}^{(k,2)}\mathbf{F}_{(1)}, \cdots, \mathbf{C}_{(1)}^{(k,n_k)}\mathbf{F}_{(1)}]$. Then, the problem can be reformulated as

(19)
$$\min_{\mathbf{W}_{k}} \frac{\lambda_{1}}{2} \|\mathbf{Z}_{1} - \mathbf{W}_{k} \mathbf{Q}_{1}\|_{F}^{2} + \frac{\lambda_{2}}{2} \|\mathbf{O}_{1} - \mathbf{W}_{k} \mathbf{F}_{1}\|_{F}^{2} + \frac{\beta_{1}}{2} \|\mathbf{W}_{k}^{*} - \mathbf{P}_{1} \mathbf{W}_{k}\|_{F}^{2} + \frac{\sigma_{1}}{2} \|\mathbf{W}_{k} - \mathbf{W}_{k,pre}\|_{F}^{2}.$$

By using $vec(\mathbf{AXB}) = (\mathbf{B}^T \otimes \mathbf{A})vec(\mathbf{X})$, and by letting $\mathbf{w}_k = vec(\mathbf{W}_k)$, we can easily rewrite the above problem as

(20)
$$\min_{\mathbf{w}_k} \frac{1}{2} ||\mathbf{u}_1 - \mathbf{D}_1 \mathbf{w}_k||_2^2,$$

where $\mathbf{u}_1 = [\sqrt{\lambda_1}vec(\mathbf{Z}_1)^T, \sqrt{\lambda_2}vec(\mathbf{O}_1)^T, \sqrt{\beta_1}vec(\mathbf{W}_k^*)^T, \sqrt{\sigma}vec(\mathbf{W}_{k,pre})^T]^T, \mathbf{D}_1 = [\sqrt{\lambda_1}(\mathbf{Q}_1^T \otimes \mathbf{I})^T, \sqrt{\lambda_2}(\mathbf{F}_1^T \otimes \mathbf{I})^T, \sqrt{\sigma}\mathbf{I}]^T$. This problem has a closed-form solution written as

(21)
$$\mathbf{w}_k = (\mathbf{D}_1^T \mathbf{D}_1)^{-1} \mathbf{D}_1^T \mathbf{u}_1.$$

4.3. \mathbf{H}_k subproblem. With the other parameters fixed, \mathbf{H}_k can be updated similarly by solving

(22)
$$\min_{\mathbf{H}_{k}} \frac{\lambda_{1}}{2} \| \mathcal{Z}^{(k)} - \mathcal{C}^{(k)} \times_{1} \mathbf{W}_{k} \times_{2} \mathbf{H}_{k} \times_{3} \mathbf{P}_{3} \mathbf{S}_{k} \|_{F}^{2} + \frac{\lambda_{2}}{2} \| \mathcal{O}^{(k)} - \mathcal{C}^{(k)} \times_{1} \mathbf{W}_{k} \times_{2} \mathbf{H}_{k} \times_{3} \mathbf{S}_{k} \|_{F}^{2} + \frac{\beta_{2}}{2} \| \mathbf{H}_{k}^{*} - \mathbf{P}_{2} \mathbf{H}_{k} \|_{F}^{2} + \frac{\sigma}{2} \| \mathbf{H}_{k} - \mathbf{H}_{k,pre} \|_{F}^{2}.$$

The above problem can be rewritten in mode-2 as follows:

(23)
$$\min_{\mathbf{H}_{k}} \frac{\lambda_{1}}{2} \|\mathbf{Z}_{2} - \mathbf{H}_{k} \mathbf{Q}_{2}\|_{F}^{2} + \frac{\lambda_{2}}{2} \|\mathbf{O}_{2} - \mathbf{H}_{k} \mathbf{F}_{2}\|_{F}^{2} + \frac{\beta_{2}}{2} \|\mathbf{H}_{k}^{*} - \mathbf{P}_{2} \mathbf{H}_{k}\|_{F}^{2} + \frac{\sigma}{2} \|\mathbf{H}_{k} - \mathbf{H}_{k,pre}\|_{F}^{2}.$$

where
$$\mathbf{Z}_2 = [\mathbf{Z}_{(2)}^{(k,1)}, \mathbf{Z}_{(2)}^{(k,2)}, \cdots, \mathbf{Z}_{(2)}^{(k,n_k)}], \ \mathbf{O}_2 = [\mathbf{O}_{(2)}^{(k,1)}, \mathbf{O}_{(2)}^{(k,2)}, \cdots, \mathbf{O}_{(2)}^{(k,n_k)}]. \ \text{In addition, } \mathbf{Q}_2 = [\mathbf{C}_{(2)}^{(k,1)} \mathbf{Q}_{(2)}, \mathbf{C}_{(2)}^{(k,2)} \mathbf{Q}_{(2)}, \cdots, \mathbf{C}_{(2)}^{(k,n_k)} \mathbf{Q}_{(2)}], \mathbf{Q}_{(2)} = (\mathbf{P}_3 \mathbf{S}_k \otimes \mathbf{W}_k)^T, \mathbf{F}_2 = [\mathbf{C}_{(2)}^{(k,1)} \mathbf{F}_{(2)}, \mathbf{C}_{(2)}^{(k,2)} \mathbf{F}_{(2)}, \cdots, \mathbf{C}_{(2)}^{(k,n_k)} \mathbf{F}_{(2)}]$$
 and $\mathbf{F}_{(2)} = (\mathbf{S}_k \otimes \mathbf{W}_k)^T$.

INVERSE PROBLEMS AND IMAGING

Similarly, letting $\mathbf{h}_k = vec(\mathbf{H}_k)$, the above problem can be easily rewritten as

(24)
$$\min_{\mathbf{h}_k} \frac{1}{2} ||\mathbf{u}_2 - \mathbf{D}_2 \mathbf{h}_k||_2^2,$$

where $\mathbf{u}_2 = [\sqrt{\lambda_1}vec(\mathbf{Z}_2)^T, \sqrt{\lambda_2}vec(\mathbf{O}_2)^T, \sqrt{\beta_2}vec(\mathbf{H}_k^*)^T, \sqrt{\sigma}vec(\mathbf{H}_{k,pre})^T]^T, \mathbf{D}_2 = [\sqrt{\lambda_1}(\mathbf{Q}_2^T \otimes \mathbf{I})^T, \sqrt{\lambda_2}(\mathbf{F}_2^T \otimes \mathbf{I})^T, \sqrt{\sigma}\mathbf{I}]^T$. This problem has a closed-form solution written as

(25)
$$\mathbf{h}_k = (\mathbf{D}_2^T \mathbf{D}_2)^{-1} \mathbf{D}_2^T \mathbf{u}_2.$$

4.4. S_k subproblem. With the other parameters fixed, S_k can be updated by solving

$$\min_{\mathbf{S}_{k}} \frac{1}{2} \| \mathcal{Y}^{(k)} - \mathcal{C}^{(k)} \times_{1} \mathbf{W}_{k}^{*} \times_{2} \mathbf{H}_{k}^{*} \times_{3} \mathbf{S}_{k} \|_{F}^{2}
+ \frac{\lambda_{1}}{2} \| \mathcal{Z}^{(k)} - \mathcal{C}^{(k)} \times_{1} \mathbf{W}_{k} \times_{2} \mathbf{H}_{k} \times_{3} (\mathbf{P}_{3} \mathbf{S}_{k}) \|_{F}^{2}
+ \frac{\lambda_{2}}{2} \| \mathcal{O}^{(k)} - \mathcal{C}^{(k)} \times_{1} \mathbf{W}_{k} \times_{2} \mathbf{H}_{k} \times_{3} \mathbf{S}_{k} \|_{F}^{2} + \frac{\sigma}{2} \| \mathbf{S}_{k} - \mathbf{S}_{k,pre} \|_{F}^{2}.$$
(26)

Furthermore, the above problem can be rewritten in mode-3 as follows:

$$\begin{split} & \min_{\mathbf{S}_{k}} \frac{1}{2} \| [\mathbf{Y}_{(3)}^{(k,1)}, \mathbf{Y}_{(3)}^{(k,2)}, \cdots, \mathbf{Y}_{(3)}^{(k,n_{k})}] - \mathbf{S}_{k} [\mathbf{C}_{(3)}^{(k,1)} \mathbf{G}_{(3)}, \mathbf{C}_{(3)}^{(k,2)} \mathbf{G}_{(3)}, \cdots, \mathbf{C}_{(3)}^{(k,n_{k})} \mathbf{G}_{(3)}] \|_{F}^{2} \\ & + \frac{\lambda_{1}}{2} \| [\mathbf{Z}_{(3)}^{(k,1)}, \mathbf{Z}_{(3)}^{(k,2)}, \cdots, \mathbf{Z}_{(3)}^{(k,n_{k})}] - \mathbf{P}_{3} \mathbf{S}_{k} [\mathbf{C}_{(3)}^{(k,1)} \mathbf{Q}_{(3)}, \mathbf{C}_{(3)}^{(k,2)} \mathbf{Q}_{(3)}, \cdots, \mathbf{C}_{(3)}^{(k,n_{k})} \mathbf{Q}_{(3)}] \|_{F}^{2} \\ & + \frac{\lambda_{2}}{2} \| [\mathbf{O}_{(3)}^{(k,1)}, \mathbf{O}_{(3)}^{(k,2)}, \cdots, \mathbf{O}_{(3)}^{(k,n_{k})}] - \mathbf{S}_{k} [\mathbf{C}_{(3)}^{(k,1)} \mathbf{F}_{(3)}, \mathbf{C}_{(3)}^{(k,2)} \mathbf{F}_{(3)}, \cdots, \mathbf{C}_{(3)}^{(k,n_{k})} \mathbf{F}_{(3)}] \|_{F}^{2} \\ & + \frac{\sigma}{2} \| \mathbf{S}_{k} - \mathbf{S}_{k,pre} \|_{F}^{2}, \end{split}$$

where $\mathbf{Y}_{(3)}^{(k,j)}, \mathbf{Z}_{(3)}^{(k,j)}, \mathbf{O}_{(3)}^{(k,j)}$ and $\mathbf{C}_{(3)}^{(k,j)}$ are mode-3 unfolding matrices of tensors $\mathcal{Y}^{(k,j)}, \mathcal{Z}^{(k,j)}, \mathcal{O}^{(k,j)}$ and $\mathcal{C}^{(k,j)}$, respectively, and $\mathbf{G}_{(3)} = ((\mathbf{P}_2\mathbf{H}_k) \otimes (\mathbf{P}_1\mathbf{W}_k))^T, \mathbf{Q}_{(3)} = \mathbf{F}_{(3)} = (\mathbf{H}_k \otimes \mathbf{W}_k)^T$.

In addition, we can denote $\mathbf{Y}_3 = [\mathbf{Y}_{(3)}^{(k,1)}, \mathbf{Y}_{(3)}^{(k,2)}, \cdots, \mathbf{Y}_{(3)}^{(k,n_k)}], \mathbf{Z}_3 = [\mathbf{Z}_{(3)}^{(k,1)}, \mathbf{Z}_{(3)}^{(k,2)}, \cdots, \mathbf{Z}_{(3)}^{(k,n_k)}],$ $\mathbf{O}_3 = [\mathbf{O}_{(3)}^{(k,1)}, \mathbf{O}_{(3)}^{(k,2)}, \cdots, \mathbf{O}_{(3)}^{(k,n_k)}], \mathbf{G}_3 = [\mathbf{C}_{(3)}^{(k,1)}\mathbf{G}_{(3)}, \mathbf{C}_{(3)}^{(k,2)}\mathbf{G}_{(3)}, \cdots, \mathbf{C}_{(3)}^{(k,n_k)}\mathbf{G}_{(3)}], \mathbf{Q}_3 = [\mathbf{C}_{(3)}^{(k,1)}\mathbf{Q}_{(3)}, \mathbf{C}_{(3)}^{(k,2)}\mathbf{Q}_{(3)}, \cdots, \mathbf{C}_{(3)}^{(k,n_k)}\mathbf{Q}_{(3)}]$ and $\mathbf{F}_3 = [\mathbf{C}_{(3)}^{(k,1)}\mathbf{F}_{(3)}, \mathbf{C}_{(3)}^{(k,2)}\mathbf{F}_{(3)}, \cdots, \mathbf{C}_{(3)}^{(k,n_k)}\mathbf{F}_{(3)}].$ Then, the problem can be reformulated as

$$\min_{\mathbf{S}_{k}} \frac{1}{2} \|\mathbf{Y}_{3} - \mathbf{S}_{k} \mathbf{G}_{3}\|_{F}^{2} + \frac{\lambda_{1}}{2} \|\mathbf{Z}_{3} - \mathbf{P}_{3} \mathbf{S}_{k} \mathbf{Q}_{3}\|_{F}^{2} + \frac{\lambda_{2}}{2} \|\mathbf{O}_{3} - \mathbf{S}_{k} \mathbf{F}_{3}\|_{F}^{2}
+ \frac{\sigma}{2} \|\mathbf{S}_{k} - \mathbf{S}_{k,pre}\|_{F}^{2}.$$
(27)

By using $vec(\mathbf{AXB}) = (\mathbf{B}^T \otimes \mathbf{A})vec(\mathbf{X})$, and by letting $\mathbf{s}_k = vec(\mathbf{S}_k)$, we can easily rewrite the above problem as

(28)
$$\min_{\mathbf{s}_k} \frac{1}{2} ||\mathbf{u}_3 - \mathbf{D}_3 \mathbf{s}_k||_2^2,$$

where $\mathbf{u}_3 = [vec(\mathbf{Y}_3)^T, \sqrt{\lambda_1}vec(\mathbf{Z}_3)^T, \sqrt{\lambda_2}vec(\mathbf{O}_3)^T, \sqrt{\sigma}vec(\mathbf{S}_{k,pre})^T]^T, \mathbf{D}_3 = [(\mathbf{G}_3^T \otimes \mathbf{I})^T, \sqrt{\lambda_1}(\mathbf{Q}_3^T \otimes \mathbf{P}_3)^T, \sqrt{\lambda_2}(\mathbf{F}_3^T \otimes \mathbf{I})^T, \sqrt{\sigma}(\mathbf{I}^T \otimes \mathbf{I})^T]^T.$

This problem has a closed-form solution written as

$$\mathbf{s}_k = (\mathbf{D}_3^T \mathbf{D}_3)^{-1} \mathbf{D}_3^T \mathbf{u}_3.$$

In order to simplify computation, we set $\mathbf{M}_3 = \mathbf{G}_3^T \otimes \mathbf{I}, \mathbf{N}_3 = \mathbf{Q}_3^T \otimes \mathbf{P}_3, \mathbf{A}_3 = \mathbf{F}_3^T \otimes \mathbf{I}$ and $\mathbf{y}_3 = vec(\mathbf{Y}_3), \mathbf{z}_3 = vec(\mathbf{Z}_3), \mathbf{o}_3 = vec(\mathbf{O}_3), \mathbf{s}_{k,pre} = vec(\mathbf{S}_{k,pre})$. Then, we can obtain

$$\begin{split} \mathbf{D}_{3}^{T}\mathbf{D}_{3} &= \mathbf{M}_{3}^{T}\mathbf{M}_{3} + \lambda_{1}\mathbf{N}_{3}^{T}\mathbf{N}_{3} + \lambda_{2}\mathbf{A}_{3}^{T}\mathbf{A}_{3} + \sigma\mathbf{I} \\ &= (\mathbf{G}_{3}^{T}\otimes\mathbf{I})^{T}(\mathbf{G}_{3}^{T}\otimes\mathbf{I}) + \lambda_{1}(\mathbf{Q}_{3}^{T}\otimes\mathbf{P}_{3})^{T}(\mathbf{Q}_{3}^{T}\otimes\mathbf{P}_{3}) \\ &+ \lambda_{2}(\mathbf{F}_{3}^{T}\otimes\mathbf{I})^{T}(\mathbf{F}_{3}^{T}\otimes\mathbf{I}) + \sigma\mathbf{I} \\ &= \mathbf{G}_{3}\mathbf{G}_{3}^{T}\otimes\mathbf{I} + \lambda_{1}\mathbf{Q}_{3}\mathbf{Q}_{3}^{T}\otimes\mathbf{P}_{3}^{T}\mathbf{P}_{3} + \lambda_{2}\mathbf{F}_{3}\mathbf{F}_{3}^{T}\otimes\mathbf{I} + \sigma\mathbf{I} \\ \mathbf{D}_{3}^{T}\mathbf{u}_{3} &= \mathbf{M}_{3}^{T}\mathbf{y}_{3} + \lambda_{1}\mathbf{N}_{3}^{T}\mathbf{z}_{3} + \lambda_{2}\mathbf{A}_{3}^{T}\mathbf{o}_{3} + \sigma\mathbf{s}_{k,pre} \\ &= vec(\mathbf{Y}_{3}\mathbf{G}_{3}^{T} + \lambda_{1}\mathbf{P}_{3}^{T}\mathbf{Z}_{3}\mathbf{Q}_{3}^{T} + \lambda_{2}\mathbf{O}_{3}\mathbf{F}_{3}^{T} + \sigma\mathbf{S}_{k,pre}). \end{split}$$

4.5. \mathbf{W}_{k}^{*} subproblem. With the other parameters fixed, \mathbf{W}_{k}^{*} can be updated by solving

$$\min_{\mathbf{W}_{k}^{*}} \frac{1}{2} \| \mathcal{Y}^{(k)} - \mathcal{C}^{(k)} \times_{1} \mathbf{W}_{k}^{*} \times_{2} \mathbf{H}_{k}^{*} \times_{3} \mathbf{S}_{k} \|_{F}^{2} + \frac{\beta_{1}}{2} \| \mathbf{W}_{k}^{*} - \mathbf{P}_{1} \mathbf{W}_{k} \|_{F}^{2}
(30) + \frac{\sigma}{2} \| \mathbf{W}_{k}^{*} - \mathbf{W}_{k,pre}^{*} \|_{F}^{2}.$$

Furthermore, the above problem can be rewritten in mode-1 as follows:

$$\begin{aligned} & \min_{\mathbf{W}_{k}^{*}} \frac{1}{2} \| [\mathbf{Y}_{(1)}^{(k,1)}, \mathbf{Y}_{(1)}^{(k,2)}, \cdots, \mathbf{Y}_{(1)}^{(k,n_{k})}] - \mathbf{W}_{k}^{*} [\mathbf{C}_{(1)}^{(k,1)} \mathbf{G}_{(1)}, \mathbf{C}_{(1)}^{(k,2)} \mathbf{G}_{(1)}, \cdots, \mathbf{C}_{(1)}^{(k,n_{k})} \mathbf{G}_{(1)}] \|_{F}^{2} \\ & + \frac{\beta_{1}}{2} | \| \mathbf{W}_{k}^{*} - \mathbf{P}_{1} \mathbf{W}_{k} \|_{F}^{2} + \frac{\sigma}{2} \| \mathbf{W}_{k}^{*} - \mathbf{W}_{k,pre}^{*} \|_{F}^{2}, \end{aligned}$$

where $\mathbf{Y}_{(1)}^{(k,j)}$ and $\mathbf{C}_{(1)}^{(k,j)}$ are mode-1 unfolding matrices of tensors $\mathcal{Y}^{(k,j)}$ and $\mathcal{C}^{(k,j)}$, respectively, and $\mathbf{G}_{(1)} = (\mathbf{S}_k \otimes \mathbf{H}_k^*)^T$. In addition, we can denote $\mathbf{Y}_1 = [\mathbf{Y}_{(1)}^{(k,1)}, \mathbf{Y}_{(1)}^{(k,2)}, \cdots, \mathbf{Y}_{(1)}^{(k,n_k)}]$ and $\mathbf{G}_1 = [\mathbf{C}_{(1)}^{(k,1)}\mathbf{G}_{(1)}, \mathbf{C}_{(1)}^{(k,2)}\mathbf{G}_{(1)}, \cdots, \mathbf{C}_{(1)}^{(k,n_k)}\mathbf{G}_{(1)}]$. Then, the problem can be reformulated as

(31)
$$\min_{\mathbf{W}_{k}^{*}} \frac{1}{2} \|\mathbf{Y}_{1} - \mathbf{W}_{k}^{*} \mathbf{G}_{1}\|_{F}^{2} + \frac{\beta_{1}}{2} \|\mathbf{W}_{k}^{*} - \mathbf{P}_{1} \mathbf{W}_{k}\|_{F}^{2} + \frac{\sigma}{2} \|\mathbf{W}_{k}^{*} - \mathbf{W}_{k,pre}^{*}\|_{F}^{2}.$$

This problem has a closed-form solution written as

(32)
$$\mathbf{W}_{k}^{*} = (\mathbf{Y}_{1}\mathbf{G}_{1}^{T} + \beta_{1}\mathbf{P}_{1}\mathbf{W}_{k} + \sigma\mathbf{W}_{k,pre}^{*})(\mathbf{G}_{1}\mathbf{G}_{1}^{T} + (\beta_{1} + \sigma)\mathbf{I})^{-1}.$$

4.6. \mathbf{H}_{k}^{*} subproblem. With the other parameters fixed, \mathbf{H}_{k}^{*} can be updated similarly by solving

(33)
$$\min_{\mathbf{H}_{k}^{*}} \frac{1}{2} \| \mathcal{Y}^{(k)} - \mathcal{C}^{(k)} \times_{1} \mathbf{W}_{k}^{*} \times_{2} \mathbf{H}_{k}^{*} \times_{3} \mathbf{S}_{k} \|_{F}^{2} + \frac{\beta_{2}}{2} \| \mathbf{H}_{k}^{*} - \mathbf{P}_{2} \mathbf{H}_{k} \|_{F}^{2} + \frac{\sigma}{2} \| \mathbf{H}_{k}^{*} - \mathbf{H}_{k,pre}^{*} \|_{F}^{2}.$$

The above problem can be rewritten in mode-2 as follows:

(34)
$$\min_{\mathbf{H}_{k}^{*}} \frac{1}{2} \|\mathbf{Y}_{2} - \mathbf{H}_{k}^{*} \mathbf{G}_{2}\|_{F}^{2} + \frac{\beta_{2}}{2} \|\mathbf{H}_{k}^{*} - \mathbf{P}_{2} \mathbf{H}_{k}\|_{F}^{2} + \frac{\sigma}{2} \|\mathbf{H}_{k}^{*} - \mathbf{H}_{k,pre}^{*}\|_{F}^{2}.$$

This problem has a closed-form solution written as

(35)
$$\mathbf{H}_{k}^{*} = (\mathbf{Y}_{2}\mathbf{G}_{2}^{T} + \beta_{2}\mathbf{P}_{2}\mathbf{H}_{k} + \sigma\mathbf{H}_{k,pre}^{*})(\mathbf{G}_{2}\mathbf{G}_{2}^{T} + (\beta_{2} + \sigma)\mathbf{I})^{-1},$$
where $\mathbf{G}_{2} = [\mathbf{C}_{(2)}^{(k,1)}\mathbf{G}_{(2)}, \mathbf{C}_{(2)}^{(k,2)}\mathbf{G}_{(2)}, \cdots, \mathbf{C}_{(2)}^{(k,n_{k})}\mathbf{G}_{(2)}], \mathbf{G}_{(2)} = (\mathbf{S}_{k}\otimes\mathbf{W}_{k}^{*})^{T} \text{ and } \mathbf{Y}_{2} = [\mathbf{Y}_{(2)}^{(k,1)}, \mathbf{Y}_{(2)}^{(k,2)}, \cdots, \mathbf{Y}_{(2)}^{(k,n_{k})}].$

4.7. P_1 subproblem. With the other parameters fixed, P_1 can be updated by solving

(36)
$$\min_{\mathbf{P}_1} \frac{\beta_1}{2} ||\mathbf{W}_k^* - \mathbf{P}_1 \mathbf{W}_k||_F^2 + \frac{\sigma}{2} ||\mathbf{P}_1 - \mathbf{P}_{1,pre}||_F^2.$$

This problem has a closed-form solution written as

(37)
$$\mathbf{P}_1 = (\beta_1 \mathbf{W}_k^* \mathbf{W}_k^T + \sigma \mathbf{P}_{1,nre})(\beta_1 \mathbf{W}_k \mathbf{W}_k^T + \sigma \mathbf{I})^{-1}.$$

4.8. P_2 subproblem. With the other parameters fixed, P_2 can be updated by solving

(38)
$$\min_{\mathbf{P}_2} \frac{\beta_2}{2} ||\mathbf{H}_k^* - \mathbf{P}_2 \mathbf{H}_k||_F^2 + \frac{\sigma}{2} ||\mathbf{P}_2 - \mathbf{P}_{2,pre}||_F^2.$$

This problem has a closed-form solution written as

(39)
$$\mathbf{P}_2 = (\beta_2 \mathbf{H}_k^* \mathbf{H}_k^T + \sigma \mathbf{P}_{2,pre})(\beta_2 \mathbf{H}_k \mathbf{H}_k^T + \sigma \mathbf{I})^{-1}.$$

INVERSE PROBLEMS AND IMAGING

4.9. $\mathcal{M}^{(k)}$ subproblem. With other parameters fixed, $\mathcal{M}^{(k)}$ can be updated by solving

(40)
$$\min_{\mathcal{M}^{(k)}} \lambda \|M_{(4)}^{(k)}\|_* + \frac{1}{2} \|\mathcal{L} + \mathcal{P}^{(k)} - \mathcal{M}^{(k)}\|_F^2,$$

where $\lambda = \frac{\mu}{\lambda_2}$ and $\mathcal{L} = \mathcal{C}^{(k)} \times_1 \mathbf{W}_k \times_2 \mathbf{H}_k \times_3 \mathbf{S}_k$, which has been proven to have the following closed-form solution:

(41)
$$\mathcal{M}^{(k)} = \text{fold}_4(V_1 S_\lambda(\Sigma) V_2^T),$$

where $V_1 \Sigma V_2^T$ is the SVD of unfold₄($\mathcal{L} + \mathcal{P}^{(k)}$) and $S_{\lambda}(\Sigma)$ is the soft thresholding operator on diagonal matrix Σ with parameters λ . The *ii*-th entry of the diagonal matrix $S_{\lambda}(\Sigma)$ is defined as

$$S_{\lambda}(\Sigma)_{ii} = \max(0, \Sigma_{ii} - \lambda).$$

4.10. $\mathcal{P}^{(k)}$ subproblem. The Lagrangian multipliers are updated by

$$\mathcal{P}^{(k)} := \mathcal{P}^{(k)} + \lambda_2 (\mathcal{L} - \mathcal{M}^{(k)}).$$

Once the dictionaries $\mathbf{W}_k, \mathbf{H}_k, \mathbf{S}_k$ and core tensors $\mathcal{C}^{(k)}$ $(k = 1, 2, \dots, K)$ are known, all overlapping HR-HSI cubes can be estimated by using equation (6) and returned to the original place to reconstruct the target HR-HSI \mathcal{X} . We summarize the proposed algorithm in Algorithm

```
Algorithm 1 (Blind Algorithm). Input: LR-HSI \mathcal{Y}, HR-MSI \mathcal{Z}, \mathbf{P}_3. Output: HR-HSI \mathcal{X}.
```

Group the similar cubes of Z and Y into cluster tensors $Z^{(k)}$ and $Y^{(k)}$ by K-means ++, initialize $\mathbf{W}_k, \mathbf{H}_k$ and \mathbf{S}_k by using Tensor factorization technique on $Z^{(k)}$ and $Y^{(k)}$, respectively, and $\mathbf{W}_k^*, \mathbf{H}_k^*$ are initialized by averaging every a (a is the scaling factor) rows of \mathbf{W}_k and \mathbf{H}_k , $k = 1, \dots, K$. For each cluster k.

```
1, \cdots, \overset{\circ}{K}. For each cluster k, repeat

step 1. Update C^{(k)} by solving (14).

step 2. Update \mathbf{W}_k by solving (21).

step 3. Update \mathbf{H}_k by solving (25).

step 4. Update \mathbf{S}_k by solving (29).

step 5. Update \mathbf{W}_k^* by solving (32).

step 6. Update \mathbf{H}_k^* by solving (35).

step 7. Update \mathbf{S}_k by solving (29).

step 8. Update \mathbf{P}_1 by solving (37).

step 9. Update \mathbf{P}_2 by solving (39).

step 10. Update \mathcal{M}^{(k)} by solving (41).

step 11. Update \mathcal{P}^{(k)} by solving (42).

until stopping criterion is satisfied.

Estimate \mathcal{X}^{(k)} by the equation (6). Reformulate \mathcal{X}^{(k)} to obtain \mathcal{X}.
```

Next, we will state the convergence result of our algorithm for $C^{(k)}$ in the following theorem. The basic convergence result can be found in several references, such as [27, 34].

Theorem 4.1. Assume $({\bf B}_1^{(k)}^*, {\bf B}_2^{(k)}^*, {\bf B}_3^{(k)}^*, {\bf C}^{(k)}^*)$ is the minimizer of problem (13). Suppose $\eta_{c_1} = \eta_{c_2} = \eta_{c_3}$, then the sequence $({\bf B}_1^{(k)}^{t+1}, {\bf B}_2^{(k)}^{t+1}, {\bf B}_3^{(k)}^{t+1}, {\bf C}^{(k)}^{t+1})$ generated by the iteration scheme (14) is convergent and $\lim_{t\to\infty} {\bf C}^{(k)}^{t+1} = {\bf C}^{(k)}^*$.

5. Numerical experiments. In this section, we numerically demonstrate the superior performance of the proposed blind HSI super-resolution model on the simulated and real HSIs. In general, the number of clusters K is set as $\frac{n}{80}$ with n the total number of cubes. The sparsity regularization parameters λ_c and μ of the proposed model are both tested over a range of parameters 10^d , d=-6,-5,-4,-3,-2,-1, and then we choose $\lambda_c=10^{-4}$ and $\mu=10^{-3}$ for all the data for simplicity. In addition, the parameter λ_1 used to balance two fidelity terms is empirically set as 10, and we simply set the algorithm parameter $\lambda_2=10^{-3}$. We compare the proposed method with several related HSI super-resolution methods: a subspace regularization method HySure [24] 1 , a coupled non-negative matrix factorization method CNMF [37] 2 and a coupled blind tensor

¹http://www.lx.it.pt/~bioucas/publications.html

²http://naotoyokoya.com/

factorization method STEREO [14] 3 . For fair comparison, all the methods are tested with the same given spectral downsampling matrix \mathbf{P}_3 , instead of estimating it as in Hysure and CNMF. Moreover, the spatial downsampling location of Hysure is given accurately and the key parameters are optimally chosen in each method. All the experiments are run under Windows 7 and MATLAB R2017a with Intel Core i5-5200U CPU@2.80GHz and 8GB memory.

5.1. Evaluation metrics. We adopt five quantitative metrics, including peak signal-to-noise ratio (PSNR), structural similarity (SSIM), root mean square error (RMSE), spectral angle mapper(SAM) and erreur relative globale adimensionnelle Synthèse (ERGAS). PSNR is easily defined based on the mean square error(MSE),

$$PSNR(\mathcal{X}, \widehat{\mathcal{X}}) = \frac{1}{S} \sum_{k=1}^{S} PSNR_k, \ PSNR_k = 10 \cdot \log_{10} \left(\frac{255^2}{MSE(\mathbf{X}_k, \widehat{\mathbf{X}}_k)} \right),$$

where \mathbf{X}_k and $\widehat{\mathbf{X}}_k$ denote the k^{th} band images of the ground-truth HSI $\mathcal{X} \in \mathbb{R}^{W \times H \times S}$ and the estimated HSI $\widehat{\mathcal{X}} \in \mathbb{R}^{W \times H \times S}$, respectively. MSE(\mathbf{X}_k , $\widehat{\mathbf{X}}_k$) is the mean squared error between \mathbf{X}_k and $\widehat{\mathbf{X}}_k$. SSIM is used for predicting the perceptual quality in the image. The SSIM of HSI is designed as the sum of SSIM_k of the k^{th} band:

$$\mathrm{SSIM}(\mathcal{X},\widehat{\mathcal{X}}) = \frac{1}{S} \sum_{k=1}^{S} \mathrm{SSIM}_k, \ \mathrm{SSIM}_k = \frac{(2\mu_{\mathbf{X}_k} \mu_{\widehat{\mathbf{X}}_k} + C_1)(2\sigma_{\mathbf{X}_k \widehat{\mathbf{X}}_k} + C_2)}{(\mu_{\mathbf{X}_k}^2 + \mu_{\widehat{\mathbf{X}}_k}^2 + C_1)(\sigma_{\mathbf{X}_k}^2 + \sigma_{\widehat{\mathbf{X}}_k}^2 + C_2)},$$

where $\mu_{\mathbf{X}_k}$ and $\mu_{\widehat{\mathbf{X}}_k}$ denote the mean value of the elements in \mathbf{X}_k and $\widehat{\mathbf{X}}_k$, respectively. $\sigma_{\mathbf{X}_k}$ and $\sigma_{\widehat{\mathbf{X}}_k}$ denote the variances of \mathbf{X}_k and $\widehat{\mathbf{X}}_k$, respectively. $\sigma_{\mathbf{X}_k\widehat{\mathbf{X}}_k}$ denotes the covariance between \mathbf{X}_k and $\widehat{\mathbf{X}}_k$. PSNR and SSIM are commonly used in imaging science to verify experimental results, and the higher the value of them, the better the image quality. RMSE is used to measure differences between \mathcal{X} and $\widehat{\mathcal{X}}$, which is defined as

$$\text{RMSE}(\mathcal{X}, \widehat{\mathcal{X}}) = \sqrt{\frac{\|\mathcal{X} - \widehat{\mathcal{X}}\|_F^2}{WHS}}.$$

The lower the RMSE, the lower the reconstruction error. In addition, SAM is defined as

$$\mathrm{SAM}(\mathcal{X}, \hat{\mathcal{X}}) = \frac{1}{WH} \sum_{i=1}^{W} \sum_{j=1}^{H} \arccos \frac{\hat{\mathbf{x}}_{ij}^T \mathbf{x}_{ij:}}{\|\hat{\mathbf{x}}_{ij:}\|_2 \|\mathbf{x}_{ij:}\|_2},$$

where \mathbf{x}_{ij} : and $\hat{\mathbf{x}}_{ij}$: represent the spectral vectors at spatial pixel (i,j) of \mathcal{X} and $\widehat{\mathcal{X}}$, respectively. SAM measures the spectral distortion between the estimated and ground-truth images, and small SAMs correspond to good spectral quality. ERGAS is defined as

$$\mathrm{ERGAS}(\mathcal{X}, \hat{\mathcal{X}}) = \frac{100}{a} \sqrt{\frac{1}{S} \sum_{k=1}^{S} \frac{\mathrm{MSE}(\mathbf{X}_{k}, \widehat{\mathbf{X}}_{k})}{\mu_{\mathbf{X}_{k}}^{2}}},$$

where a is spatial downsampling factor, and small ERGAS values indicate good fusion performance.

5.2. Simulated HSI super-resolution. In this section, we test the effectiveness of the proposed method on the CAVE database [38], which contains 32 hyperspectral images, each with 31 spectral bands, ranging from 400nm to 700nm with resolution 10nm, and a spatial resolution of 512 \times 512. We use the CAVE database as the ground truth image \mathcal{X} , and simulate the LR-HSI \mathcal{Y} by employing an 8×8 uniform blur or a 7×7 Gaussian blur with 0 mean and standard deviation 3 to \mathcal{X} before downsampling with scaling factor 8 along each of the spatial directions. The HR-MSI \mathcal{Z} is generated by degrading the hyperspectral image \mathcal{X} using a spectral transform matrix \mathbf{P}_3 based on the response of a Nikon D700 camera ⁴. The average values of each of the five quantitative measures for each compared HSI super-resolution methods on all 32 scenes have been listed in Table 1. It can be seen that the proposed method leads to better quantitative results than all the other three methods. For better comparison, we also show the SAM values of 32 images with uniform blur corresponding to different methods in Figure 2. We can observe that the proposed method (red color) has the lowest SAM values for all images in CAVE database. In Figure 3, we compare their visual performance in peppers (cartoon image) and flowers (texture image) of the CAVE

³We thank the authors of [14] for providing their codes.

⁴https://www.maxmax.com/nikon_d700_study.htm

dataset with Gaussian blur. The first and third columns of Figure 3 show the constructed images of the peppers at the 8^{th} band and the flowers at the 14^{th} band, respectively. Their corresponding absolute error images are shown in the second and fourth columns. Blue color corresponds to low error. We observe that all competing methods keep spatial structures well, but the proposed method leads to the lowest reconstruction errors and the best visual quality in restoring both smooth areas and texture regions. More details can be observed from the zoomed in patches in Figure 3. The proposed method performs better than other test methods both quantitatively and qualitatively.

TABLE 1. Comparison on the average values of each of the five quantitative measures on 32 scenes from CAVE dataset with scaling factor 8.

Methods	PSNR	SSIM	RMSE	SAM	ERGAS			
Uniform blur								
CNMF[37]	43.052	0.985	2.299	5.934	1.224			
Hysure[24]	41.461	0.975	2.702	10.737	1.497			
STEREO[14]	39.680	0.946	3.611	12.212	1.898			
Proposed	45.332	0.987	1.822	4.969	0.984			
Gaussian blur								
CNMF[37]	42.258	0.981	2.511	6.578	1.329			
Hysure[24]	41.961	0.977	2.541	10.310	1.425			
STEREO[14]	39.542	0.945	3.658	12.251	1.923			
Proposed	45.206	0.987	1.847	4.983	0.995			

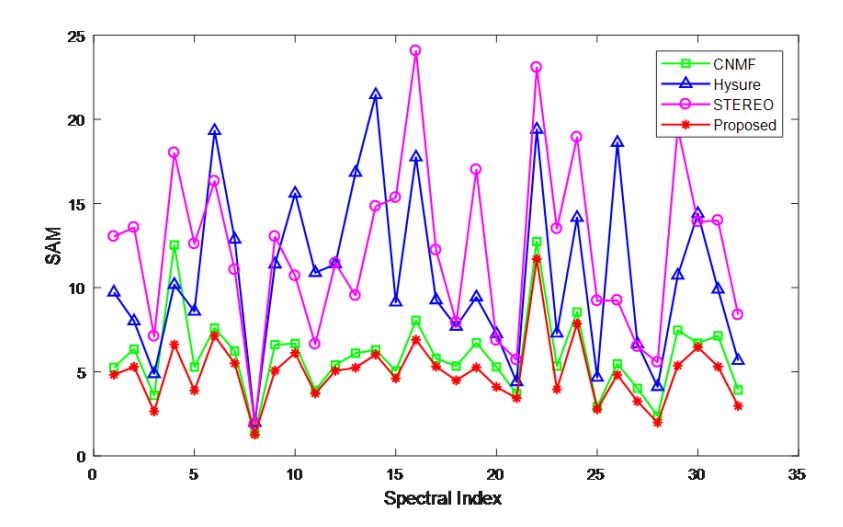


FIGURE 2. The SAMs of all competing methods on CAVE dataset with uniform blur

5.3. Hyperspectral remote sensing image super-resolution. In this section, we mainly demonstrate the performance of the proposed method on the Indian Pines image [30]. The image was obtained by the Airbornes Visible/Infrared Imaging Spectrometer (AVIRIS) sensor, and the whole image contains 145×145 pixels and 224 spectral bands in the wavelength range 400-2500nm. In our experiments, a subimage of size $120 \times 120 \times 224$ is used as the ground truth image \mathcal{X} . The HR-MSI \mathcal{Z} with six bands is degenerated by using LANDSAT sensor, and each spectral band captures the 450-520nm, 520-600nm, 630-690nm, 760-900nm, 1550-1750nm, 2080-2350nm information of

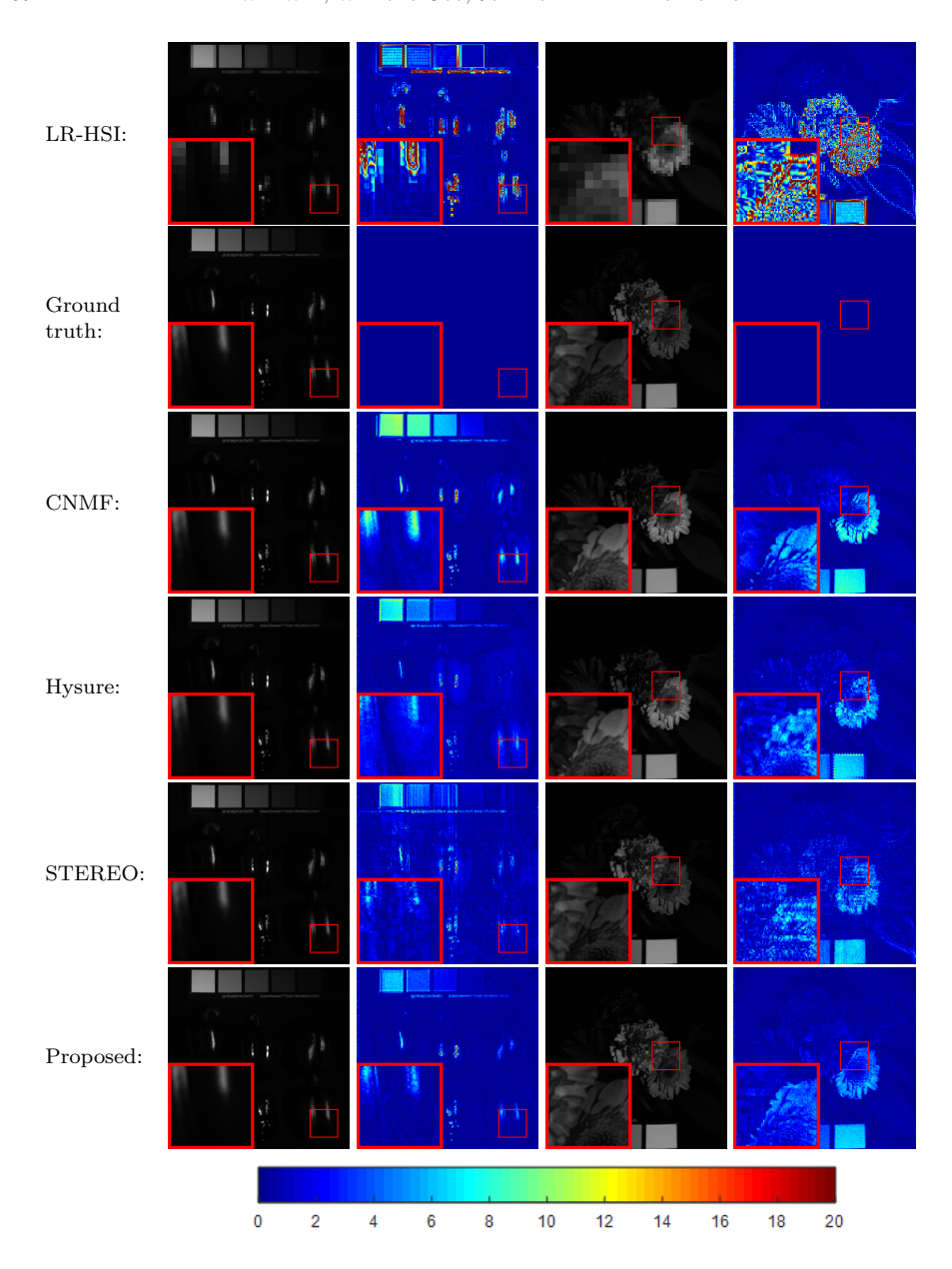


FIGURE 3. The reconstructed images and the corresponding error images of fake and real peppers at the 8^{th} band and flowers at the 14^{th} band with Gaussian blur and scaling factor 8.

the hyperspectral image \mathcal{X} , respectively. The LR-HSI \mathcal{Y} is generated as the spatial degradation manner for the CAVE dataset. Both uniform blur and Gaussian blur are tested with scaling factor 8. The quantitative results obtained with different test methods on the Indian Pines image are compared in Table 2. We can clearly see that the proposed method significantly outperforms other methods with respective to all the quantitative measures, especially for the case of Gaussian blur. Figure 4 shows the reconstructed images and the corresponding absolute error images of all the competing methods at the 60^{th} and 130^{th} bands (the bright one and the dark one). We observe

that the proposed method still leads to best results among all test methods. In addition, we report a numerical evidence for the convergence of the proposed algorithm. The functional energy curve as a function of the iteration for the first similar cluster with uniform blur is shown in Figure 5. We can observe that it rapidly stabilizes in a few iteration numbers.

TABLE 2. The performance comparison of the methods on the Indian Pines image with scaling factor 8.

Methods	PSNR	SSIM	RMSE	SAM	ERGAS			
Uniform blur								
CNMF[37]	42.866	0.978	2.557	2.394	9.406			
Hysure[24]	45.232	0.984	1.891	1.701	9.389			
STEREO[14]	48.212	0.985	1.267	1.225	9.405			
Proposed	51.441	0.993	0.928	0.888	9.368			
Gaussian blur								
CNMF[37]	42.740	0.977	2.599	2.430	9.409			
Hysure[24]	45.927	0.986	1.703	1.547	9.384			
STEREO[14]	47.050	0.981	1.510	1.413	9.438			
Proposed	51.326	0.993	0.950	0.904	9.369			

5.4. Experimental results on remote sensing data corrupted by Gaussian noise. In this section, we consider to verify the robustness of the proposed model to Gaussian noise by using the Pavia data [8]. The whole image contains 610×340 pixels and 115 spectral bands, acquired by the reflective optics system imaging spectrometer (ROSIS). In our experiments, only a subimage of size $256 \times 256 \times 93$ was chosen after removing the water vapor absorption bands. To generate the noisy LR-HSI \mathcal{Y} , the ground truth image \mathcal{X} is downsampled by first using the uniform blur with scaling factor 8 as before, and we then add Gaussian noise. The noisy HR-MSI \mathcal{Z} is firstly simulated by degrading \mathcal{X} using the IKONOS-like reflectance spectral response filter [33] and then adding Gaussian noise. We use SNRh and SNRm to represent SNR of the simulated noisy LR-HSI and HR-MSI, respectively. Table 3 lists the quantitative results of all compared methods on the Pavia image with different Gaussian noise. The visual comparison results are shown in Figure 6. The first and second columns show the reconstructed images and the corresponding error images at the 45^{th} band of the Pavia image with SNRh 30dB and SNRm 35dB, respectively. The third and forth columns show the reconstructed images and the corresponding error images at the 75^{th} band of the Pavia image with SNRh 35dB and SNRm 40dB, respectively. It can be observed that the proposed model has lower reconstruction errors and better quantitative results than the other methods.

TABLE 3. The performance comparison of noisy cases on the Pavia image with uniform blur and scaling factor 8.

Methods	PSNR	SSIM	RMSE	SAM	ERGAS			
SNRh=35dB, SNRm=40dB								
CNMF[37]	37.958	0.982	3.335	2.790	0.958			
Hysure[24]	42.573	0.987	2.278	2.420	0.584			
STEREO[14]	37.307	0.951	3.715	4.022	1.039			
Proposed	43.731	0.989	1.848	1.944	0.497			
SNRh=30dB, SNRm=35dB								
CNMF[37]	37.694	0.979	3.439	2.885	0.979			
Hysure[24]	41.541	0.982	2.338	2.553	0.644			
STEREO[14]	35.584	0.932	4.401	4.829	1.252			
Proposed	42.097	0.981	2.158	2.349	0.604			

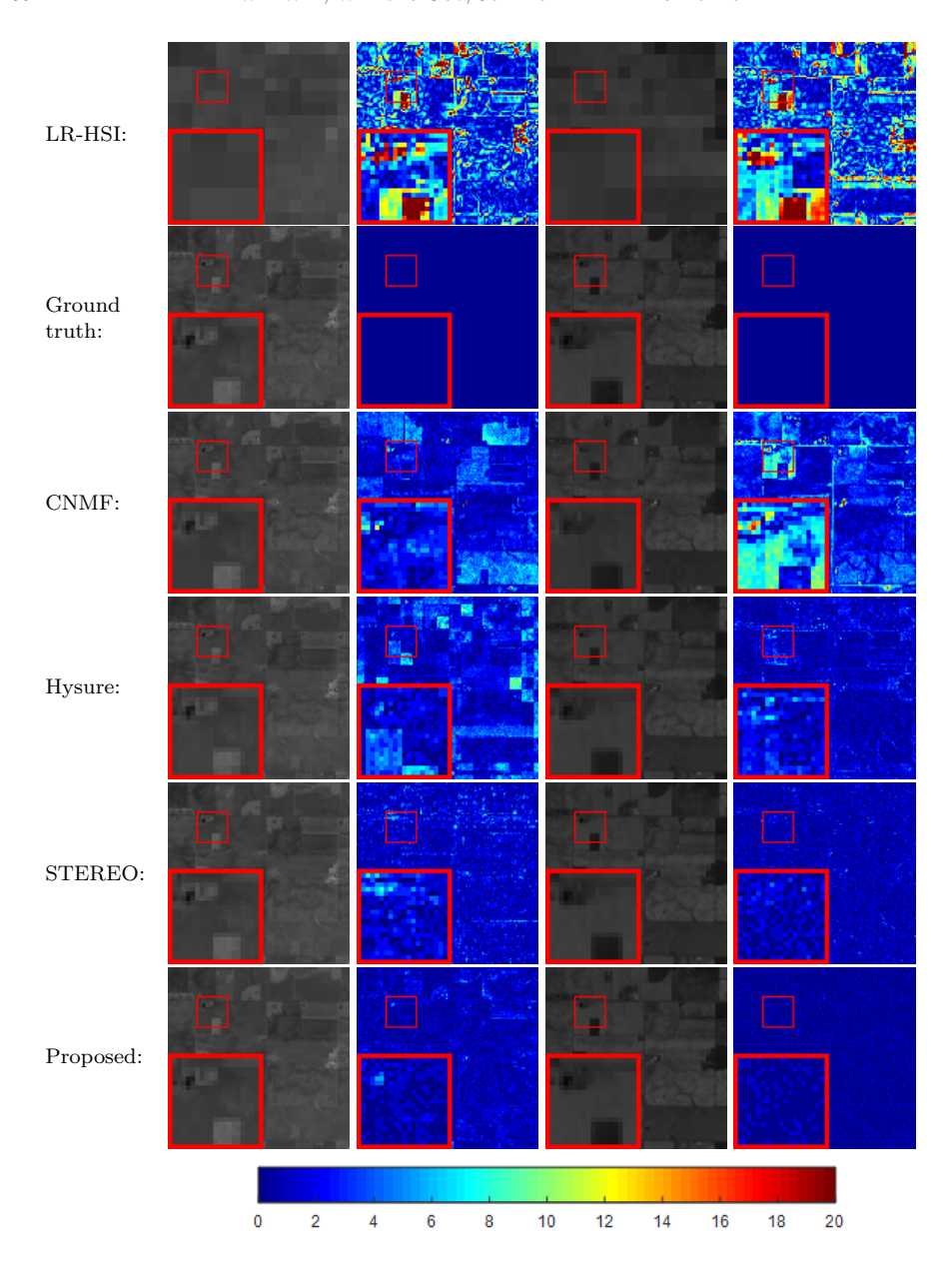


FIGURE 4. The reconstructed images and the corresponding error images of the Indian Pines image at the 60^{th} and 130^{th} bands with uniform blur and scaling factor 8.

6. Conclusion. Motivated by the fact that the spatial degradation operators are usually unknown in practice, this work presents a novel blind HSI super-resolution approach based on non-local sparse tensor factorization. We first group similar 3D image cubes of the LR-HSI $\mathcal Y$ and HR-MSI $\mathcal Z$ into some clusters and then organize them as a 4D tensor for each cluster. The sparse tensor regularization is designed according to the sparse prior and low-rank of the targeted 4D tensors. By using the tensor factorization technique for each similar cluster, the problem of HSI super-resolution can be reformulated to estimate the dictionaries of three modes and their corresponding

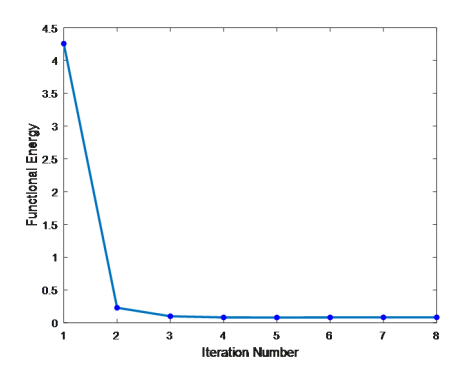


Figure 5. The functional energy curve for the proposed algorithm.

core tensors. To solve the proposed method efficiently, we present a proximal ADMM based algorithm. Numerical experiments on both simulated and real image data demonstrate that the proposed model can provide some state-of-the-art results in HSI super-resolution.

Acknowledgment. Wei Wan is supported by the China Scholarship Council (No. 201706040141). Weihong Guo's research is partially supported by NSF under grant DMS-1521582. Jun Liu and Haiyang Huang are supported by The National Key Research and Development Program of China (2017YFA0604903). Jun Liu is also partly supported by The National Natural Science Foundation of China (No. 11871035). We thank Professor Wotao Yin from UCLA for the discussion on algorithm convergence analysis.

REFERENCES

- N. Akhtar, F. Shafait and A. Mian, Bayesian sparse representation for hyperspectral image super resolution, *IEEE Computer Vision and Pattern Recognition (CVPR)*, (2015), 3631–3640.
- [2] J. M. Bioucas-Dias, A. Plaza, G. Camps-Valls, P. Scheunders, N. Nasrabadi and J. Chanussot, Hyperspectral remote sensing data analysis and future challenges, *IEEE Geoscience and Remote Sensing Magazine*, 1 (2013), 6–36.
- [3] J. M. Bioucas-Dias and A. Plaza, Hyperspectral unmixing: Geometrical, statistical, and sparse regression-based approaches, *Image and Signal Processing for Remote Sensing XVI*, (2010), 354–379.
- [4] Y. Chang, L. Yan, H. Fang, S. Zhong and Z. Zhang, Weighted Low-Rank Tensor Recovery for Hyperspectral Image Restoration, ARXIV, 2017.
- [5] C. F. Caiafa and A. Cichocki, Computing sparse representations of multidimensional signals using kronecker bases, *Neural Computation*, **25** (2013), 186–220.
- [6] W. Dong, F. Fu, G. Shi, X. Cao, J. Wu, G. Li and X. Li, Hyperspectral image super-resolution via non-negative structured sparse representation, *IEEE Transactions on Image Processing*, 25 (2016), 2337–2352.
- [7] R. Dian, L. Fang and S. Li, Hyperspectral image super-resolution via non-local sparse tensor factorization, IEEE Conference on Computer Vision and Pattern Recognition (CVPR), (2017).
- [8] F. Dell"Acqua, P. Gamba, A. Ferrari, J. A. Palmason, J. A. Benediktsson and K. Arnason, Exploiting spectral and spatial information in hyperspectral urban data with high resolution, IEEE Geoscience and Remote Sensing Letters, 1 (2004), 322–326.
- [9] H. Fan, Y. Chen, Y. Guo, H. Zhang and G. Kuang, Hyperspectral image restoration using low-rank tensor recovery, IEEE Journal of Selected Topics in Applied Earth Observations and Remote Sensing, 10 (2017), 4589–4604.
- [10] A. F. H. Goetz, Three decades of hyperspectral remote sensing of the earth: A personal view, Remote Sensing of Environment, 113 (2009), S5–S16.

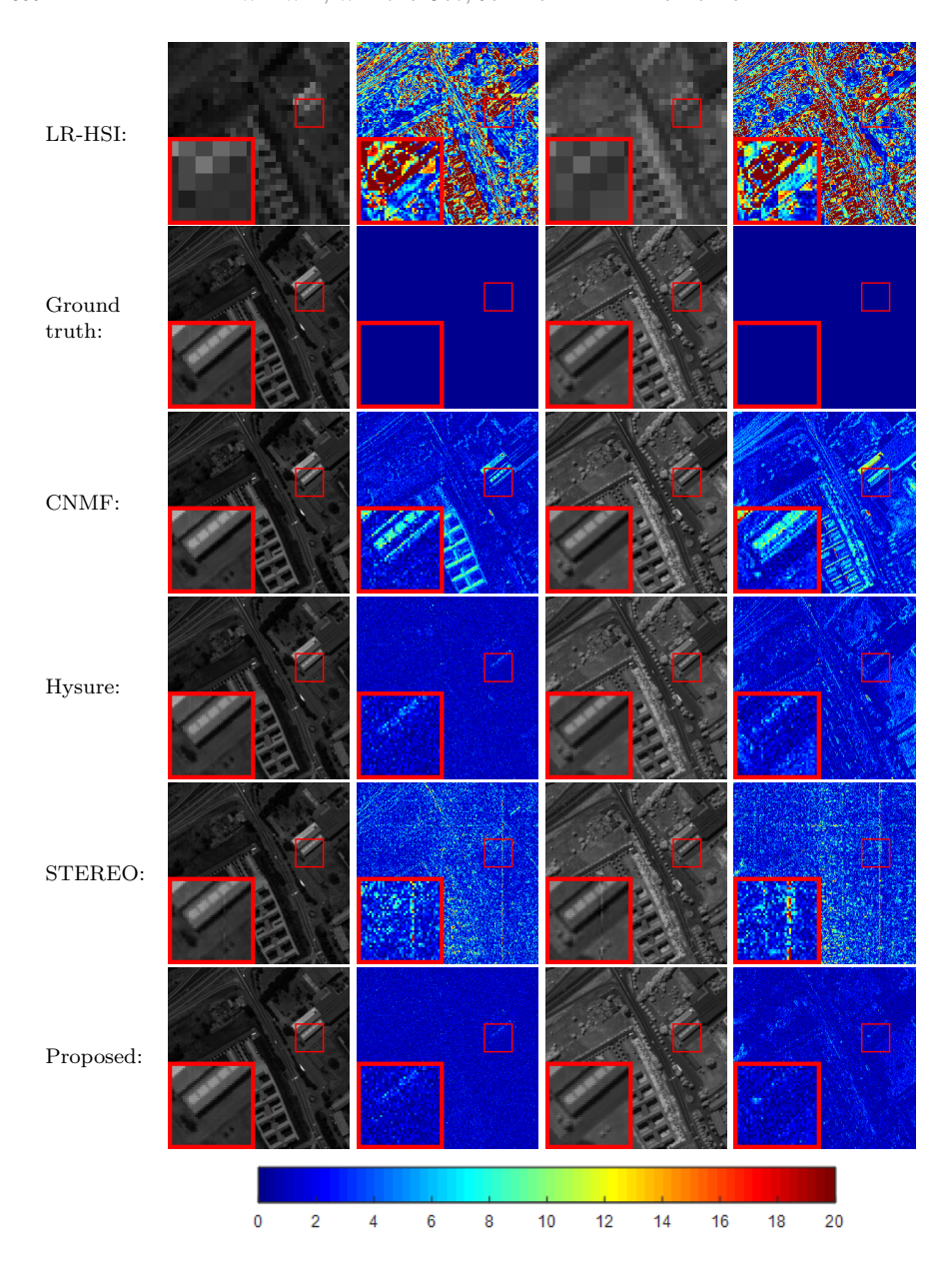


FIGURE 6. The reconstructed images and the corresponding error images of the Pavia image at the 45^{th} and 75^{th} bands with uniform blur and scaling factor 8.

^[11] C. Jia and Y. Fu, Low-rank tensor subspace learning for RGB-D action recognition, IEEE Transactions on Image Processing, 25 (2016), 4641–4652.

^[12] C. Jia, M. Shao and Y. Fu, Sparse canonical temporal alignment with deep tensor decomposition for action recognition, *IEEE Transactions on Image Processing*, 26 (2017), 738–750.

^[13] R. Kawakami, J. Wright, Y. W. Tai and Y. Matsushita, High-resolution hyperspectral imaging via matrix factorization, Computer Vision and Pattern Recognition (CVPR), (2011), 2329– 2336.

- [14] C. I. Kanatsoulis, X. Fu, N. D. Sidiropoulos and W. K. Ma, Hyperspectral super-resolution: A coupled tensor factorization approach, *IEEE Transactions on Signal Processing*, 66 (2018), 6503–6517.
- [15] T. G. Kolda and B. W. Bader, Tensor decompositions and applications, Siam Review, 51 (2009), 455–500.
- [16] W. Li, G. Wu, F. Zhang and Q. Du, Hyperspectral image classification using deep pixel-pair features, IEEE Transactions on Geoscience and Remote Sensing, 55 (2016), 844–853.
- [17] X. Liu, W. Xia, B. Wang and L. Zhang, An approach based on constrained nonnegative matrix factorization to unmix hyperspectral data, *IEEE Transactions on Geoscience and Remote Sensing*, 49 (2011), 757–772.
- [18] S. Li, R. Dian, L. Fang and J. M. Bioucas-Dias, Fusing hyperspectral and multispectral images via coupled sparse tensor factorization, *IEEE Transactions on Image Processing*, 27 (2018), 4118–4130.
- [19] M. J. Montag and H. Stephani, Hyperspectral unmixing from incomplete and noisy data, Journal of Imaging, 2 (2016), p7.
- [20] J. Ma, H. Zhou, J. Zhao, Y. Cao, J. Jiang and J. Tian, Robust feature matching for remote sensing image registration via locally linear transforming, *IEEE Transactions on Geoscience* and Remote Sensing, 53 (2015), 6469–6481.
- [21] H. V. Nguyen, A. Banerjee and R. Chellappa, Tracking via object reflectance using a hyperspectral video camera, IEEE Computer Society Conference on Computer Vision and Pattern Recognition - Workshops, (2010).
- [22] Y. Peng, D. Meng, Z. Xu, C. Cao, Y. Yang and B. Zhang, Decomposable nonlocal tensor dictionary learning for multispectral image denoising, *IEEE Conference on Computer Vision* and Pattern Recognition, (2014).
- [23] Y. Qian, F. Xiong, S. Zeng, J. Zhou and Y. Y. Tang, Matrix-vector nonnegative tensor factorization for blind unmixing of hyperspectral imagery, *IEEE Transactions on Geoscience* and Remote Sensing, 55 (2017), 1776–1792.
- [24] M. Simoes, J. M. Bioucas-Dias, L. B. Almeida and J. Chanussot, A convex formulation for hyperspectral image superresolution via subspace-based regularization, *IEEE Transactions* on Geoscience and Remote Sensing, 53 (2014), 3373–3388.
- [25] S. Soltani, M. E. Kilmer and P. C. Hansen, A tensor-based dictionary learning approach to tomographic image reconstruction, BIT Numerical Mathematics, 56 (2016), 1425–1454.
- [26] Y. Tarabalka, J. Chanussot and J. A. Benediktsson, Segmentation and classification of hyperspectral images using minimum spanning forest grown from automatically selected markers, IEEE Transactions on Systems, Man, and Cybernetics, 40 (2010), 1267–1279.
- [27] X. C. Tai and C. Wu, Augmented Lagrangian method, dual methods and split Bregman iteration for ROF model, *International Conference on Scale Space and Variational Methods* in Computer Vision, (2009), 502–513.
- [28] M. Uzair, A. Mahmood and A. Mian, Hyperspectral face recognition using 3D-DCT and partial least squares, *BMVC*, **10** (2013), 1–57.
- [29] M. Uzair, A. Mahmood and A. Mian, Hyperspectral face recognition with spatiospectral information fusion and PLS regression, *IEEE Transactions on Image Processing*, 24 (2015), 1127–1137.
- [30] G. Vane, R. O. Green, T. G. Chrien, H. T. Enmark, E. G. Hansen and W. M. Porter, The airborne visible/infrared imaging spectrometer (AVIRIS), Remote Sensing of Environment, 44 (1993), 127–143.
- [31] E. Wycoff, T. H. Chan, K. Jia, W. K. Ma and Y. Ma, A non-negative sparse promoting algorithm for high resolution hyperspectral imaging, IEEE International Conference on Acoustics, Speech and Signal Processing (ICASSP), (2013), 1409–1413.
- [32] Q. Wei, J. M. Bioucas-Dias, N. Dobigeon and J. Y. Tourneret, Hyperspectral and multispectral image fusion based on a sparse representation, *IEEE Transactions on Geoscience and Remote Sensing*, 53 (2015), 3658–3668.
- [33] Q. Wei, N. Dobigeon and J. Y. Tourneret, Fast fusion of multi-band images based on solving a Sylvester equation, *IEEE Transactions on Image Processing*, **24** (2015), 4109–4121.
- [34] W. Wan, J. Liu and H. Huang, Local block operators and TV regularization based image inpainting, Inverse Problems and Imaging, 12 (2018), 1389–1410.
- [35] Q. Xie, Q. Zhao, D. Meng, Z. Xu, S. Gu, W. Zuo and L. Zhang, Multispectral images denoising by intrinsic tensor sparsity regularization, IEEE Conference on Computer Vision and Pattern Recognition (CVPR), (2016).

- [36] Q. Xie, Q. Zhao, D. Meng and Z. Xu, Kronecker-basis-representation based tensor sparsity and its applications to tensor recovery, *IEEE Transactions on Pattern Analysis and Machine Intelligence*, 40 (2018), 1888–1902.
- [37] N. Yokoya, T. Yairi and A. Iwasaki, Coupled nonnegative matrix factorization unmixing for hyperspectral and multispectral data fusion, *IEEE Transactions on Geoscience and Remote Sensing*, 50 (2012), 528–537.
- [38] F. Yasuma, T. Mitsunaga, D. Iso and S. K. Nayar, Generalized assorted pixel camera: post-capture control of resolution, dynamic range, and spectrum, *IEEE Transactions on Image Processing*, 19 (2010), 2241–2253.
- [39] L. Zhang, W. Wei, C. Bai, Y. Gao and Y. Zhang, Exploiting clustering manifold structure for hyperspectral imagery super-resolution, *IEEE Transactions on Image Processing*, 27 (2018), 5969–5982.
- [40] Z. Zhang, E. Pasolli, M. M. Crawford and J. C. Tilton, An active learning framework for hyperspectral image classification using hierarchical segmentation, *IEEE Journal of Selected Topics in Applied Earth Observations and Remote Sensing*, 9 (2016), 640–654.
- [41] H. Zhang, J. Li, Y. Huang and L. Zhang, A nonlocal weighted joint sparse representation classification method for hyperspectral imagery, *IEEE Journal of Selected Topics in Applied Earth Observations and Remote Sensing*, 7(2014), 2056–2065.
- [42] H. Zhang, H. Zhai, L. Zhang and P. Li, Spectral-spatial sparse subspace clustering for hyperspectral remote sensing images, IEEE Transactions on Geoscience and Remote Sensing, 54 (2016), 3672–3684.

Received June 2019; revised October 2019.

E-mail address: weiwan@mail.bnu.edu.cn

E-mail address: wxg49@case.edu E-mail address: jliu@bnu.edu.cn E-mail address: hhywsg@bnu.edu.cn